AD_____

Award Number: W81XWH-09-1-0204

TITLE: Inhibitors of Fatty Acid Synthase for Prostate Cancer

PRINCIPAL INVESTIGATOR: Steven J. Kridel, Ph.D.

CONTRACTING ORGANIZATION: Wake Forest University
Winston-Salem, NC 27157

REPORT DATE: May 2010

TYPE OF REPORT: Annual

PREPARED FOR: U.S. Army Medical Research and Materiel Command
Fort Detrick, Maryland 21702-5012

DISTRIBUTION STATEMENT: Approved for Public Release;
Distribution Unlimited

The views, opinions and/or findings contained in this report are those of the author(s) and should not be construed as an official Department of the Army position, policy or decision unless so designated by other documentation.

REPORT DOCUMENTATION PAGE

Form Approved
OMB No. 0704-0188

The public reporting burden for this collection of information is estimated to average 1 hour per response, including the time for reviewing instructions, searching existing data sources, gathering and maintaining the data needed, and completing and reviewing the collection of information. Send comments regarding this burden estimate or any other aspect of this collection of information, including suggestions for reducing the burden, to Department of Defense, Washington Headquarters Services, Directorate for Information Operations and Reports (0704-0188), 1215 Jefferson Davis Highway, Suite 1204, Arlington, VA 22202-4302. Respondents should be aware that notwithstanding any other provision of law, no person shall be subject to any penalty for failing to comply with a collection of information if it does not display a currently valid OMB control number.

PLEASE DO NOT RETURN YOUR FORM TO THE ABOVE ADDRESS.

1. REPORT DATE *(DD-MM-YYYY)*	2. REPORT TYPE	3. DATES COVERED *(From - To)*
5/31/2010	Annual	01 May 2009-30 April 2010

4. TITLE AND SUBTITLE

Inhibitors of Fatty Acid Synthase for Prostate Cancer"

5a. CONTRACT NUMBER

5b. GRANT NUMBER

W81XWH-09-1-0204

5c. PROGRAM ELEMENT NUMBER

6. AUTHOR(S)

Steven J. Kridel, Ph.D.

Email: skridel@wfubmc.edu

5d. PROJECT NUMBER

5e. TASK NUMBER

5f. WORK UNIT NUMBER

7. PERFORMING ORGANIZATION NAME(S) AND ADDRESS(ES)

Wake Forest University Health Sciences
Medical Center Boulevard
Winston-Salem, NC 27157

8. PERFORMING ORGANIZATION REPORT NUMBER

9. SPONSORING/MONITORING AGENCY NAME(S) AND ADDRESS(ES)

U.S. Army Medical Research and Materiel Command
Fort Detrick, MD 21702-5012

10. SPONSOR/MONITOR'S ACRONYM(S)

11. SPONSOR/MONITOR'S REPORT NUMBER(S)

12. DISTRIBUTION/AVAILABILITY STATEMENT

Approved for public release; distribution unlimited

13. SUPPLEMENTARY NOTES

14. ABSTRACT

Fatty acid synthase (FASN), the enzyme that synthesizes fatty acid in cells, is over-expressed in prostate cancer and a potential therapeutic target. We have identified several novel chemical scaffolds with potential to inhibit FASN. An extensive series of anti-FASN pharmacophores has been synthesized and characterized for their ability to inhibit recombinant FASN, FASN activity in tumor cells, and to kill prostate cancer cell lines. The best inhibitors have increased potency over other FASN inhibitors, including orlistat, the prototype FASN thioesterase inhibitor. The current studies represent a significant advancement of the development of FASN inhibitors and moves a step closer to translating FASN inhibitors into the clinic.

15. SUBJECT TERMS

fatty acid synthase, thioesterase, inhibitors, drug development

16. SECURITY CLASSIFICATION OF:			17. LIMITATION OF ABSTRACT	18. NUMBER OF PAGES	19a. NAME OF RESPONSIBLE PERSON
a. REPORT	b. ABSTRACT	c. THIS PAGE			USAMRMC
U	U	U	UU	44	19b. TELEPHONE NUMBER *(Include area code)*

Table of Contents

Introduction

The purpose of the current research proposal is to optimize chemical scaffolds that were identified as potential inhibitors of fatty acid synthase (FASN), specifically the thioesterase (TE) domain. It is based on a series of observation by our group and others than FASN represents a valuable drug target. Using a iterative scheme of *in silico* design, activity=based screening and structural analyses we identified a series of novel pharmacophores with inhibitory activity against FASN. This proposal had three specific aims. They were 1) To optimize Compound A through structure-based design, chemical syntheses and *in vitro* testing, 2) To determine the toxicological and pharmacokinetic properties of the most promising Compound A analog(s), and 3) To test the efficacy of Compound A analog(s) in mouse xenograft models of human prostate cancer. During the course of the initial funding period significant progress has been made in optimizing initial compounds, developing new compounds and synthetic strategies, and optimizing potential FASN inhibitors for future therapeutic development. The progress of our multidisciplinary group is summarized below.

Body

In this first project year we focused on Lead Series development starting from two structural families identified as hits in high-throughput screening. Our molecular design and medicinal chemistry efforts have led to the synthesis of more than seventy (70) fully characterized compounds representing six structural classes: 5,6-quinoline-diones, naphthylene-1,4-diones, 1,4-benzoquinones, 1,4-hydroquinones, benzo[*d*]isoxazole-4,7-diones and 1*H*-indazole-4,7-diones. The novel members of these classes are the subject matter of three provisional patent applications. All salient data collected, thus far on these compounds is summarized in Appendix A. Significantly we have identified three compounds (TPI-403, TPI-417 and TPI-421) as candidates for further optimization, and *in vivo* assessment against prostate cancer.

I. Pharmacological and *in vitro* data for TPI-403, TPI-417 and TPI-421

Based on our medicinal chemistry efforts and data collected thus far, the 1*H*-indazole-4,7-dione scaffold appears to be a flexible template for further optimization. Figure 1 summarizes data for the compounds we have selected for *in vivo* assessment and further optimization.

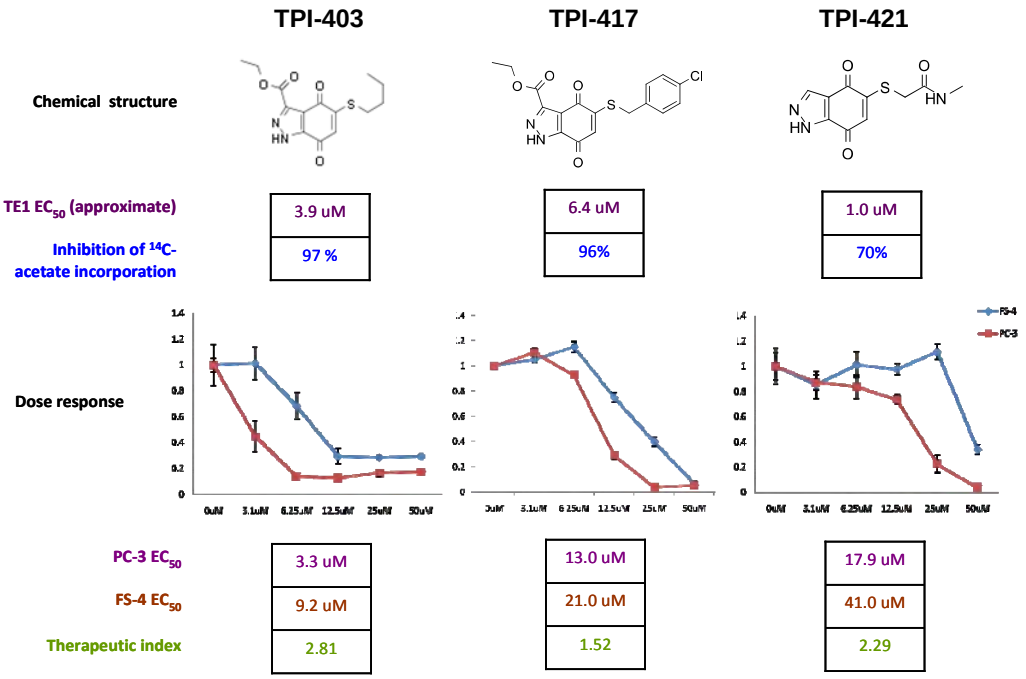

Figure 1- Lead Series Data Summary

Key: PC-3, prostate cancer cells; FS-4, normal fibroblast (control cell line); therapeutic index, {FS-4 EC_{50}}/{ FS-4 EC_{50}}

II. Further optimization strategy for TPI-403, TPI-417 and TPI-421

Further optimization of this series centers on two themes: (1) increasing affinity at TE and (2) increasing solubility in aqueous media. The former goal will also likely lead to a desired increase in therapeutic index of the series (defined here as $EC_{50(\text{normal cells})}/EC_{50(\text{cancer cells})}$).The structure-activity relationships thus far indicate that a wide variety of substituents are accommodated in Regions A and B of the 1*H*-indazole-4,7-diones scaffold. These regions are depicted in Figure 2.

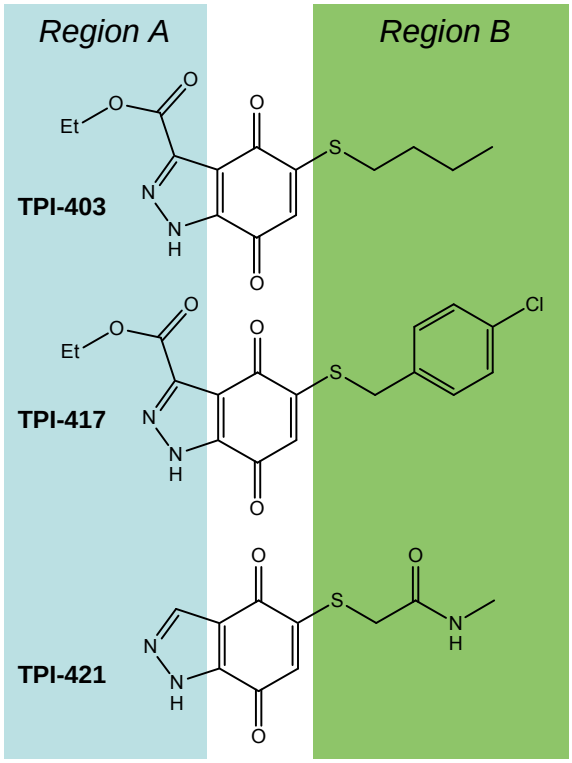

Figure 2- 1*H*-indazole-4,7-dione optimization regions

The further optimization plan for Region A is summarized in Figure 3 and will take advantage of the fact that the 5 position of the 1,4-dihydroquinone intermediate (blue structure, Figure 3) is highly susceptible to nucelophilic attack. In addition, well-established Diels-Alder chemistry will be used to create additional fused ring structures (structures 3d and 3f). Other key targets include: the introduction of various substituents (R1) into the indazole ring of structure 3a; and coupling of various aldehydes and α,β-unsaturated ethers to the 5 position of the quinine under acidic conditions to yield compounds like 3c and 3e.

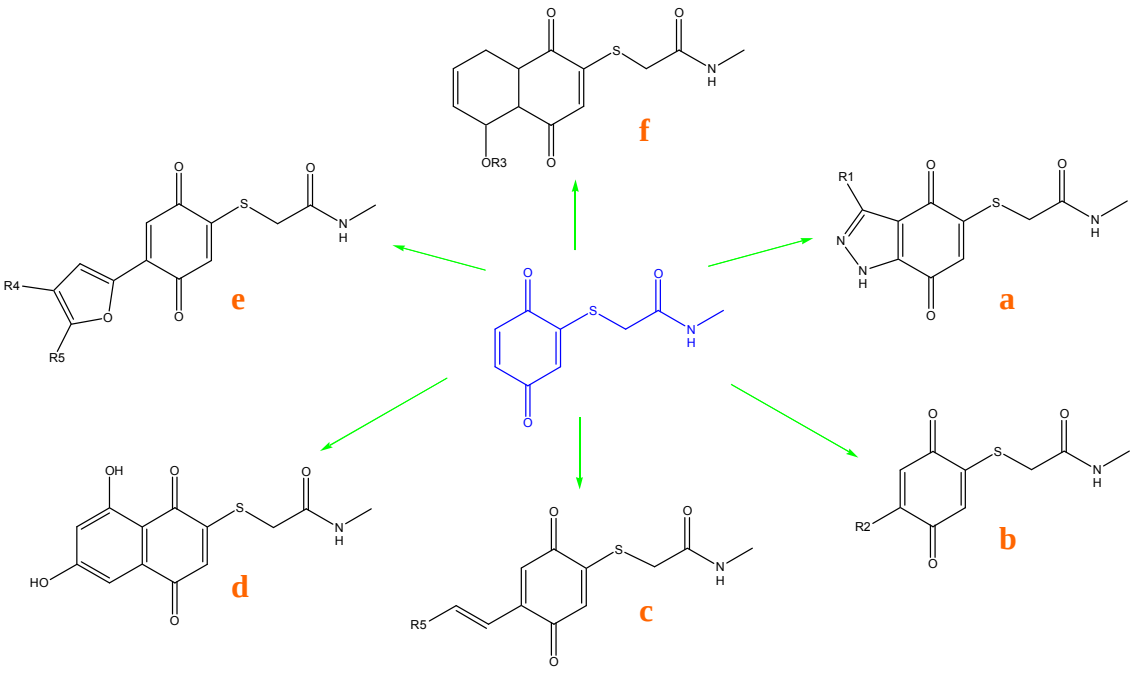

Figure 3- Region A optimization strategy for TPI-403, TPI-417 and TPI-421

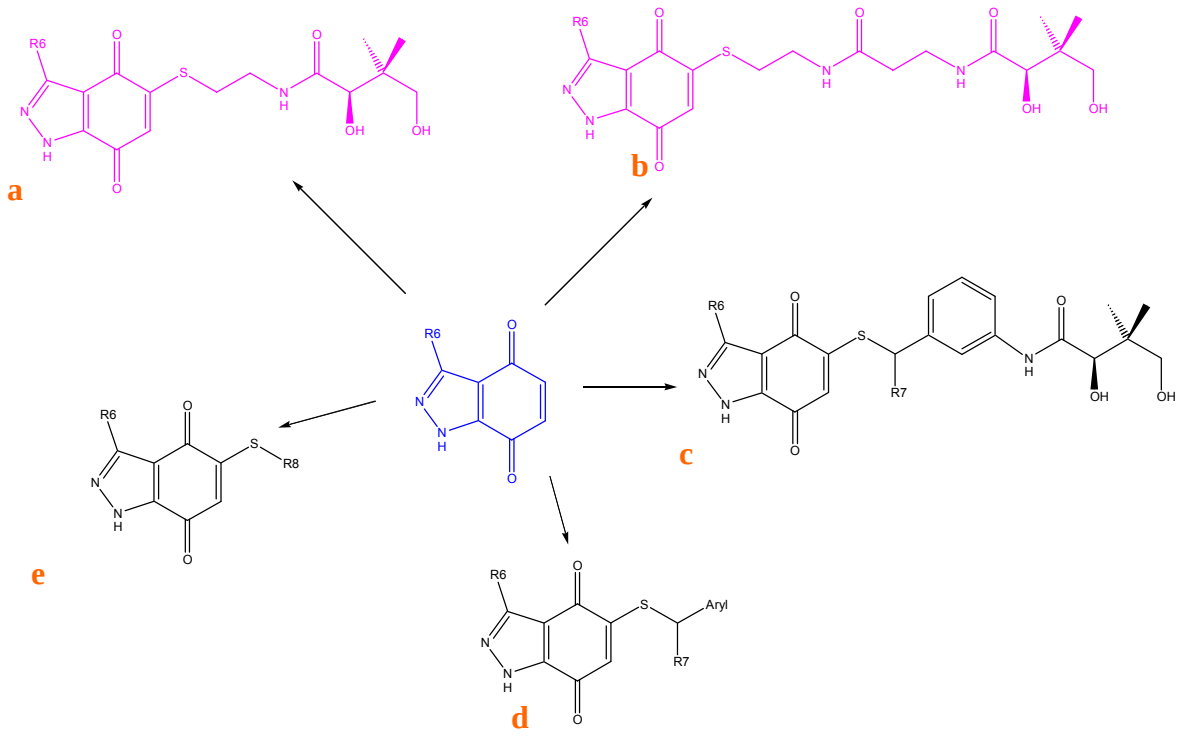

Figure 4- Region B optimization strategy for TPI-403, TPI-417 and TPI-421

The proposed further optimization of Region B, is shown in Figure 4. Here we will take advantage of crystallographic and docking data generated by our laboratories. Together these data demonstrate that substituting a pantetheine moiety onto the 1*H*-indazole-4,7-diones position of the 1*H*-indazole-4,7-dione scaffold (blue structure, Figure 4) would preserve the likely binding mode of the quinone near the catalytic triad of TE while packing the pantetheine channel, which is a unique feature of TE. We surmise that the introduction of a pantetheine moiety in a favorable orientation will not only significantly increase TE affinity and solubility, but will also increase specificity of the series toward the target. Why? Because pantetheine is a cofactor used exclusively for fatty acid synthesis, which is an absolute requirement of epithelial cancer cells and is also known to correlate with tumor aggressiveness. Examples of pantetheine -like target compounds are shown in Figure 4: structures 4a and 4b; structure 4c is an analog of TPI-417 that attempts to preserve the aromatic moiety adjacent to the indazole ring, while introducing key features of pantetheine.

Backup Compounds and Other Findings

III. 5,6-quinoline-diones

Based on our finding that the Nanosyn library compound containing the 5,6-quinoline-dione moiety (TPI-100, see Appendix A for structure) inhibits recombinant FASN TE and cancer cell growth, we pursued development of novel analogs of this 5,6-quinolinedione. Following the synthetic scheme shown in Figure 5 we were able to synthesize 10 5,6-quinoline-dione analogs. While structure-activity relationships indicated a clear trend towards a more optimal biological profile, we turned our attention toward the promising and easily synthesized 1,4-naphthoquinones and 1,4-benzoquinones.The chemistry of the 5,6-quinoline-diones have proven to be challenging due to low yields and lack of ‘generalizability’. The overall synthesis up to the hydroxyquinoline stage (structure *d*) is efficient and gives high yields overall, but the critical oxidation step (*d* → *f*) provided only marginal yields and did not work with many of the amines (*e*) of interest.

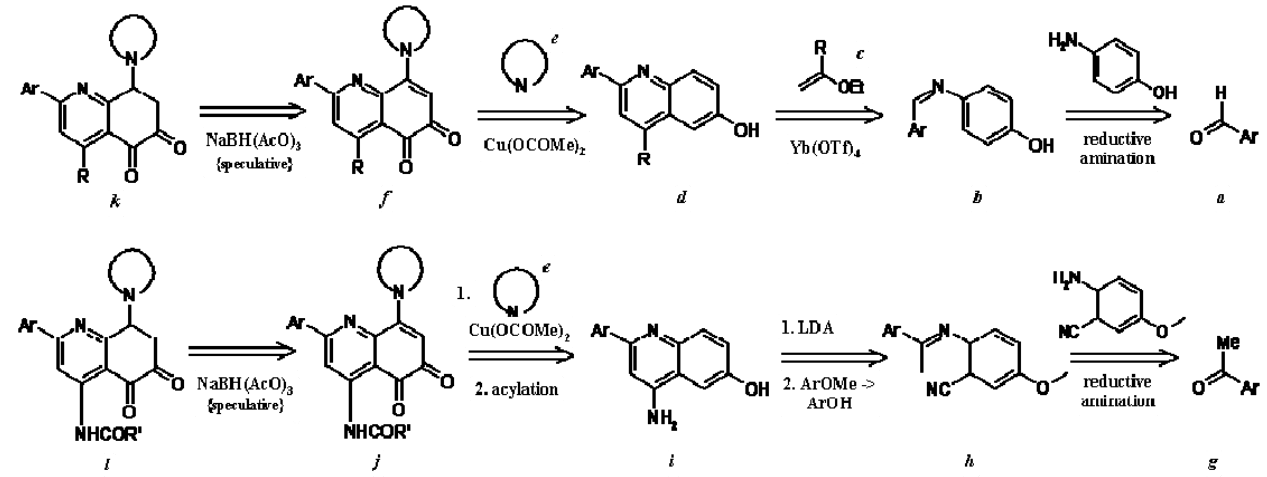

Figure 5- Synthetic strategy for 5,6-quinoline-diones

We have devised an alternative strategy that will hopefully lead to the facile development of 5,6-quinoline-diones as well as additional 1,4-benzoquinones. The overall approach is shown in Figure 6. Using this strategy, we will focus on the further optimization of TPI-107 analogs as a strategy for developing backup compounds.

IV. 1,4-naphthoquinones and 1,4-benzoquinones As mentioned above, high-throughput screening has identified two 1,4-naphthoquinones, TPI-400 and TPI-500 (see Appendix A for structures) initially analogs of these compounds were developed using the synthesis shown in Figure 7. It is worth noting that TPI-400 proved difficult to synthesize; no attempts were made to synthesize NS-500. One analog (TPI-501) was made as an attempt to reduce the chemical reactivity of the lead compound; unfortunately the pharmacological profile of the compound was very poor. A search of literature compounds and natural products led us to screen numerous 1,4-quinone containing compounds. As a result, we discovered that the natural product juglone (see Appendix A) is a potent inhibitor of TE1. One analog of juglone was synthesized (TPI-404), with the aims of making an analog with less chemical reactivity, but again, the introduction of the N-morpholinyl group was not favored.

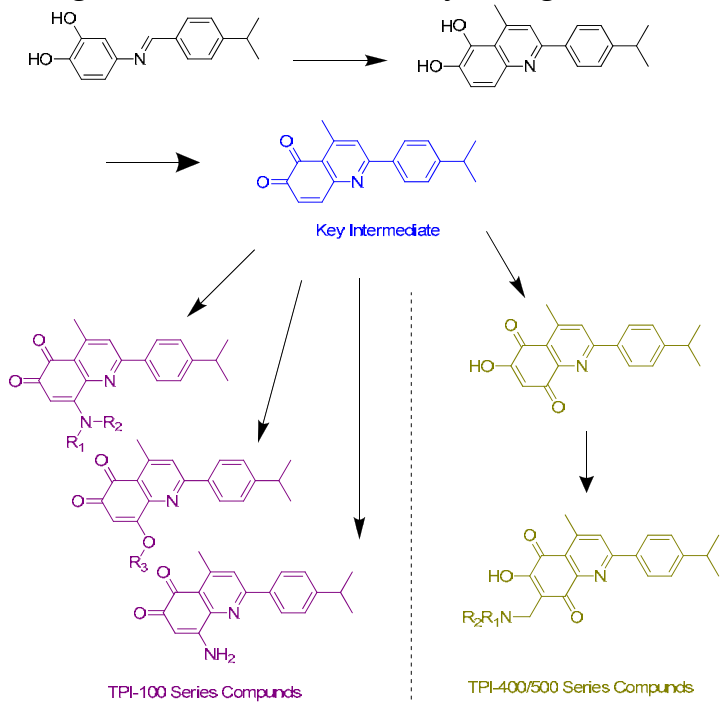

During the coarse of this work we also determined that the intellectual property space around the naphthylene-1,4-dione series is rather limited, thus we opted to find alternative scaffolds like the and 1*H*-indazole-4,7-diones described above. We also pursued the development of the closely related benzo[*d*]isoxazole-4,7-diones but we were unable to determine and efficient methodology to construct the fused isoxazole ring, nor were we able to identify an efficient process to oxidize the benzo[*d*]isoxazole-4,7-diol (TPI-401) to yield the desired product.

Figure 6- Future strategy for synthesis of 5,6-quinoline-diones

Key Research Accomplishments:

- Synthesis and characterization of more than 70 novel FASN inhibitor scaffolds. (see Appendix A)
- Optimization of FASN inhibitors of novel chemotypes
- Development of new synthetic strategies and avenues to generate FASN inhibitors

Reportable Outcomes:

Manuscripts

1. DeFord-Watts, L.M., Mintz, A. and **Kridel, S.J**., The Potential of ^{11}C-acetate PET for Monitoring the Fatty Acid Synthesis Pathway in Tumors (2010) *Current Pharmaceutical Biotechnology, Accepted*

Funding received, based on this award

None

Conclusion

As detailed in the body of this annual report, we have synthesized a significant library of potential FASN inhibitors. These results highlight the significant effort that has been put forth as well as the hurdles that have been overcome. These results will be important for the continued development of potential FASN inhibitors.

So what does this body of knowledge contribute? Several academic laboratories and pharma companies are developing inhibitors against FASN. The work presented in this report highlight design and optimization of novel FASN inhibitors. This will contribute to the development of FAS inhibitors and provide an avenue toward the translation of FAS inhibitors into the clinic for potential use in treating men with prostate cancer.

Compound Structure	TPI Number	recombinant thioesterase %Inhibition (10μM) TE1	recombinant thioesterase %Inhibition (10μM) TE2	approx, IC_{50} TE1 (μM)	approx, IC_{50} TE2 (μM)	% inhibition of ^{14}C-acetate incorp. PC3 cells	cell survival, MTS assay (IC_{50}) tumor cells PC3	cell survival, MTS assay (IC_{50}) tumor cells DU-145	cell survival, MTS assay (IC_{50}) normal cells FS-4	therapeutic index FS-4/PC3
5,6-quinolinediones										
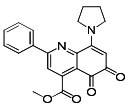	TPI-00100-00-A (NS-1456)	20.21	22.87	NA	NA	89.3	2.36	2.93	4.2	**1.78**
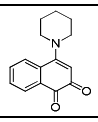	TPI-00101-00-A	2.64	8.83	NA	NA	ND	6.4	6.36	ND	ND
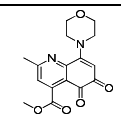	TPI-00102-00-A	17.27	14.45	NA	NA	ND	ND	ND	ND	ND
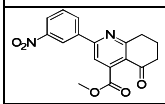	TPI-00103-00-A	1.59	11.39	NA	NA	ND	>10	>10	ND	ND
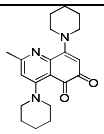	TPI-00104-00-A	0.00	12.04	NA	NA	ND	ND	ND	ND	ND
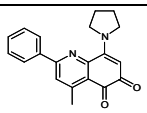	TPI-00105-00-A	9.20	17.59	NA	NA	34	> 25	> 25	ND	ND
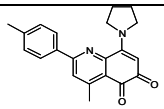	TPI-00106-00-A	37.72	42.72	NA	NA	31	> 25	20.1	16.7	ND
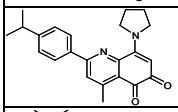	TPI-00107-00-A	51.68	54.24	11.59	13.78	49	18.2	14.33	9.4	0.52
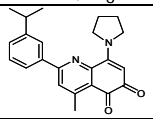	TPI-00108-00-A	21.26	26.36	NA	NA	23	> 25	> 25	ND	ND
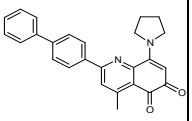	TPI-00109-00-A	30.25	26.80	NA	NA	7	> 25 uM	> 25 uM	ND	ND
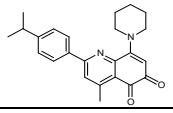	TPI-00110-00-A	28.01	46.00	NA	NA	ND	ND	ND	ND	ND
1,4-benzoquinones & 1,4-hydroquinones										
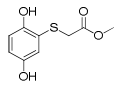	TPI-00600-00-A	85.94	96.72	7.27	NA	56.3	29.2	>50	9.5	0.33
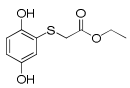	TPI-00601-00-A	94.42	96.05	7.05	NA	65.7	32.2	>50	20.8	0.65
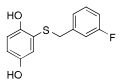	TPI-00605-00-A	30.62	46.98	NA	NA	26.7	ND	ND	ND	ND
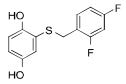	TPI-00606-00-A	10.10	14.34	NA	NA	20.3	ND	ND	ND	ND

Compound Structure	TPI Number	recombinant thioesterase %Inhibition (10μM) TE1	recombinant thioesterase %Inhibition (10μM) TE2	approx, IC_{50} TE1 (μM)	approx, IC_{50} TE2 (μM)	% inhibition of ^{14}C-acetate incorp. PC3 cells	cell survival, MTS assay (IC_{50}) tumor cells PC3	cell survival, MTS assay (IC_{50}) tumor cells DU-145	cell survival, MTS assay (IC_{50}) normal cells FS-4	therapeutic index FS-4/PC3
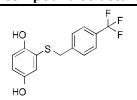	TPI-00607-00-A	45.23	19.65	NA	NA	34.3	ND	ND	ND	ND
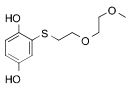	TPI-00608-00-A	35.37	93.22	NA	NA	86.2	22.4	>50	>50	ND
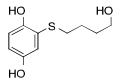	TPI-00609-00-A	78.46	96.16	NA	NA	89.6	23	>50	32.4	**1.41**
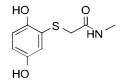	TPI-00611-00-A	31.33	8.42	NA	NA	24.5	ND	ND	ND	ND
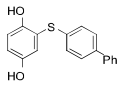	TPI-00612-00-A	0.00	47.84	NA	NA	6.25	ND	ND	ND	ND
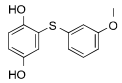	TPI-00613-00-A	13.21	70.02	NA	NA	18.9	ND	ND	ND	ND
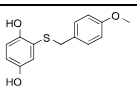	TPI-00614-00-A	37.05	89.56	NA	NA	35.2	ND	ND	ND	ND
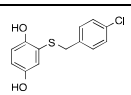	TPI-00615-00-A	18.19	NA	NA	NA	44.6	ND	ND	ND	ND
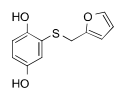	TPI-00616-00-A	95.72	95.19	NA	NA	46.7	ND	ND	ND	ND
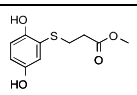	TPI-00618-00-A	22.84	90.89	NA	NA	63.6	ND	ND	ND	ND
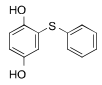	TPI-00619-00-A	18.68	85.27	NA	NA	27.7	ND	ND	ND	ND
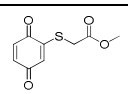	TPI-00602-00-A	100.00	100.00	1.19	NA	33.3	37.3	>50	40	**1.07**
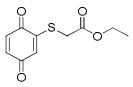	TPI-00603-00-A	100.00	100.00	1.51	NA	16	>50	>50	>50	ND
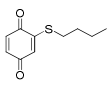	TPI-00604-00-A	100.00	100.00	NA	NA	ND	ND	ND	ND	ND
	TPI-00610-00-A	98.76	99.33	6.45	0.85	11.2	ND	ND	ND	ND
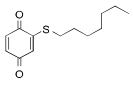	TPI-00617-00-A	99.24	98.94	6.24	0.36	45	ND	ND	ND	ND
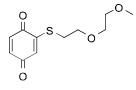	TPI-00620-00-A	98.13	98.88	1.70	0.12	91.4	20.8	ND	41.7	**2.00**

Compound Structure	TPI Number	recombinant thioesterase %Inhibition (10μM) TE1	recombinant thioesterase %Inhibition (10μM) TE2	recombinant thioesterase approx, IC_{50} TE1 (μM)	recombinant thioesterase approx, IC_{50} TE2 (μM)	% inhibition of ^{14}C-acetate incorp. PC3 cells	cell survival, MTS assay (IC_{50}) tumor cells PC3	cell survival, MTS assay (IC_{50}) tumor cells DU-145	cell survival, MTS assay (IC_{50}) normal cells FS-4	therapeutic index FS-4/PC3
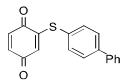	TPI-00621-00-A	100.00	100.00	1.06	0.17	23.4	ND	ND	ND	ND
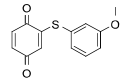	TPI-00622-00-A	100.00	100.00	0.70	0.18	11.4	ND	ND	ND	ND
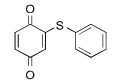	TPI-00623-00-A	100.00	100.00	1.16	0.20	9.25	ND	ND	ND	ND
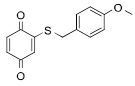	TPI-00624-00-A	100.00	100.00	1.34	0.42	57.7	33	ND	20	0.61
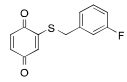	TPI-00625-00-A	100.00	100.00	1.10	0.25	64.3	22	ND	40	**1.82**
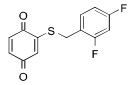	TPI-00626-00-A	100.00	99.70	1.09	0.40	42.2	ND	ND	ND	ND
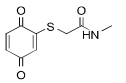	TPI-00627-00-A	100.00	99.49	1.08	0.10	66.4	19	ND	37.5	**1.97**
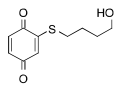	TPI-00628-00-A	100.00	97.81	1.16	0.23	53.7	>50	ND	>50	ND
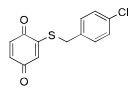	TPI-00629-00-A	100.00	100.00	1.08	0.24	50	ND	ND	ND	ND
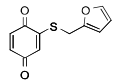	TPI-00630-00-A	100.00	100.00	1.55	0.34	61.85	ND	ND	ND	ND
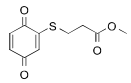	TPI-00631-00-A	100.00	100.00	1.44	0.11	91.9	>50	ND	42	ND
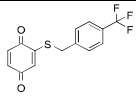	TPI-00632-00-A	100.00	100.00	1.35	0.36	49.05	ND	ND	ND	ND
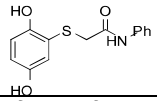	TPI-00633-00-A	76.13	98.99	NA	NA	94.2	24.3	ND	38	**1.56**
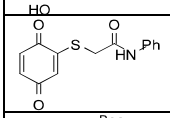	TPI-00634-00-A	100.00	100.00	NA	NA	69.7	24	ND	38	**1.58**
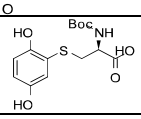	TPI-00635-00-A	28.21	9.88	NA	NA	0	>50	ND	>50	ND
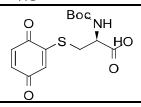	TPI-00636-00-A	81.39	100.00	NA	NA	0	>50	ND	>50	ND
naphthylene-1,4-diones, benzo[d]isoxazole-4,7-diones & 1H-indazole-4,7-diones										
	juglone	100.00	100.00	0.09	0.07	95.6	6.4	8.7	5.49	0.86

Compound Structure	TPI Number	recombinant thioesterase %Inhibition (10μM) TE1	recombinant thioesterase %Inhibition (10μM) TE2	recombinant thioesterase approx, IC_{50} TE1 (μM)	recombinant thioesterase approx, IC_{50} TE2 (μM)	% inhibition of ^{14}C-acetate incorp. PC3 cells	cell survival, MTS assay (IC_{50}) tumor cells PC3	cell survival, MTS assay (IC_{50}) tumor cells DU-145	cell survival, MTS assay (IC_{50}) normal cells FS-4	therapeutic index FS-4/PC3
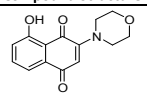	TPI-00404-00-A	29.00	43.00	NA	NA	ND	ND	ND	ND	ND
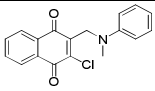	TPI-00400-00-A (NS-4390)	22.48	61.70	NA	NA	ND	29	>25	25.29	0.87
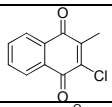	TPI-00500-01-C (NS-4393)	100.00	100.00	1.08	0.41		18.75	19.2	ND	ND
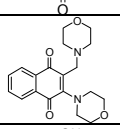	TPI-00501-01-A	44.28	34.75	NA	NA		ND	ND	ND	ND
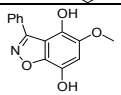	TPI-00401-00-A	40.00	55.88	NA	NA	29.1	33	>50	ND	ND
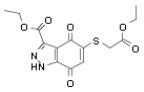	TPI-00402-00-A	66.63	95.73	2.35	0.56	90.4	18.75	40	20.9	**1.11**
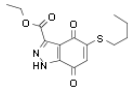	TPI-00403-00-A	69.35	79.27	3.90	2.42	97 (IC_{50} = 6.75 μM)	3.25	15.6	9.15	**2.82**
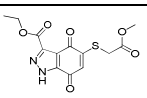	TPI-00405-00-A	69.52	96.82	2.78	0.41	ND	ND	ND	ND	ND
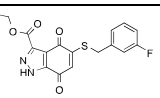	TPI-00406-00-A	73.64	96.01	NA	NA	37.7	ND	ND	ND	ND
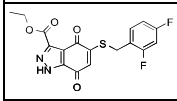	TPI-00407-00-A	65.96	94.89	NA	NA	37.8	ND	ND	ND	ND
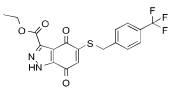	TPI-00408-00-A	67.87	96.18	NA	NA	89.9	18.5	ND	22.5	**1.22**
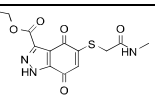	TPI-00409-00-A	53.50	92.17	NA	NA	0	ND	ND	ND	ND
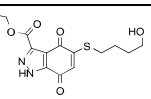	TPI-00410-00-A	59.61	91.67	NA	NA	1.85	ND	ND	ND	ND
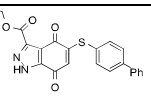	TPI-00411-00-A	70.51	97.43	NA	NA	0.75	ND	ND	ND	ND
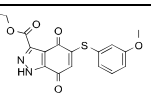	TPI-00412-00-A	81.63	97.98	NA	NA	9.95	ND	ND	ND	ND
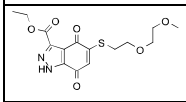	TPI-00413-00-A	50.23	94.78	NA	NA	20.2	ND	ND	ND	ND
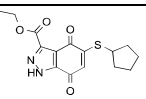	TPI-00414-00-A	52.21	86.40	NA	NA	92.4	25	ND	33	**1.32**
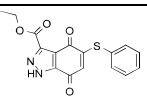	TPI-00415-00-A	79.69	97.46	NA	NA	7.05	ND	ND	ND	ND

Compound Structure	TPI Number	recombinant thioesterase %Inhibition (10μM) TE1	recombinant thioesterase %Inhibition (10μM) TE2	recombinant thioesterase approx, IC_{50} TE1 (μM)	recombinant thioesterase approx, IC_{50} TE2 (μM)	% inhibition of ^{14}C-acetate incorp. PC3 cells	cell survival, MTS assay (IC_{50}) tumor cells PC3	cell survival, MTS assay (IC_{50}) tumor cells DU-145	cell survival, MTS assay (IC_{50}) normal cells FS-4	therapeutic index FS-4/PC3
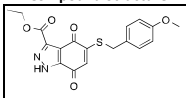	TPI-00416-00-A	64.31	96.49	NA	NA	89.9	25.8	ND	33	**1.28**
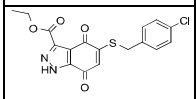	TPI-00417-00-A	74.81	97.85	NA	NA	96.1	13.8	ND	21	**1.52**
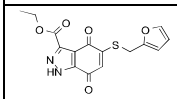	TPI-00418-00-A	65.54	95.92	NA	NA	92.2	31.7	ND	37	**1.17**
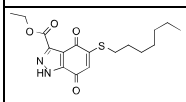	TPI-00419-00-A	66.19	95.79	NA	NA	67.95	32	ND	50	**1.56**
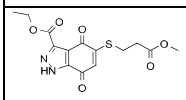	TPI-00420-00-A	61.96	95.35	NA	NA	68.5	37.5	ND	42	**1.12**
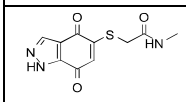	TPI-00421-00-A	100.00	100.00	1.02	NA	70	17.9	ND	41	**2.29**
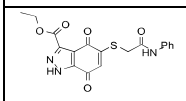	TPI-00422-00-A	22.92	86.76	NA	NA	0	48	ND	>50	ND
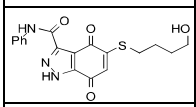	TPI-00423-00-A	79.75	97.99	NA	NA	87.25	20	ND	25	**1.25**
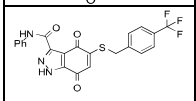	TPI-00424-00-A	92.59	100.00	NA	NA	0	27	ND	50	**1.85**
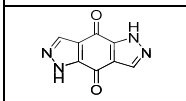	TPI-00425-00-A	0.00	73.61	NA	NA	11.1	ND	ND	ND	ND
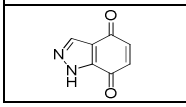	TPI-00426-00-A	48.37	79.24	NA	NA	30.1	ND	ND	ND	ND

The Potential of ^{11}C-acetate PET for Monitoring the Fatty Acid Synthesis Pathway in Tumors

Abstract

Positron emission tomography (PET) is a molecular imaging modality that provides the opportunity to rapidly and non-invasively visualize tumors derived from multiple organs. In order to do so, PET utilizes radiotracers, such as ^{18}F-FDG and ^{11}C-acetate, whose uptake coincides with altered metabolic pathways within tumors. Increased expression and activity of enzymes in the fatty acid synthesis pathway is a frequent hallmark of cancer cells. As a result, this pathway has become a prime target for therapeutic intervention. Although multiple drugs have been developed that both directly and indirectly interfere with fatty acid synthesis, an optimal means to assess their efficacy is lacking. Given that ^{11}C-acetate is directly linked to the fatty acid synthesis pathway, this probe provides a unique opportunity to monitor lipogenic tumors by PET. Herein, we review the relevance of the fatty acid synthesis pathway in cancer. Furthermore, we address the potential utility of ^{11}C-acetate PET in imaging tumors, especially those that are not FDG-avid. Last, we discuss several therapeutic interventions that could benefit from ^{11}C-acetate PET to monitor therapeutic response in patients with certain types of cancers.

Keywords: ^{11}C-acetate, fatty acid synthesis, FDG, lipid, metabolism, positron emission tomography

Running Title: PET analysis of fatty acid synthesis

Introduction

In recent years the interest in tumor cell metabolism has been reinvigorated. Advances in pathobiology, molecular biology, genomics, animal models of cancer, and technology platforms

have enhanced our knowledgebase significantly. Similarly, the development of targeted therapies and the advent of personalized medicine have provided the opportunity for cross-pollination between basic and clinical sciences. One area that has seen a surge in interest is the imaging of tumor cell metabolism through positron emission tomography (PET). The utility of PET lies in its non-invasive nature and ability to yield rapid feedback for tumor staging or therapeutic response. Significant strides have been made to connect tumor biology to clinical disease through PET. The development of multiple radiotracers with potential to image different metabolic states or pathways has further enhanced the ability to detect tumors and monitor targeted therapies [1]. In this review, the potential of ^{11}C-acetate PET to image fatty acid synthesis and detect tumors, as well as its connection to tumor pathobiology is discussed.

Tumor metabolism and the lipogenic phenotype

The most basic principle of cancer is that a group of cells autonomously proliferate out of sync with the organism's needs and the cell's microenvironment. To this end, a tumor cell is dependent on its ability to gain ample access to energy and substrate precursors for assembly into new macromolecules. These seemingly basic requirements of a cancer cell lead to an elaborate reprogramming of normal metabolic pathways that are essential for the proliferation and survival of tumor cells [2]. Understanding how and when these fundamental processes are altered will provide an opportunity to improve the treatment and surveillance of cancer.

One of the primary abnormalities of most cancer cells includes their heightened dependence on glucose. In the early 1920's, Otto Warburg observed that even in the presence of sufficient oxygen (an environment favorable for oxidative phosphorylation) cancer cells will preferentially utilize glycolysis to metabolize glucose [3]. Although this phenomenon may seem

counterintuitive, aerobic glycolysis, also known as the Warburg effect, is thought to provide cancer cells with several survival benefits [4-5]. First, the reliance on glucose for energy relieves a tumor cell of oxygen dependence in a hypoxic microenvironment. Furthermore, heightened glucose consumption provides an abundant source of energy that can be rapidly utilized as needed. Perhaps just as important as a source of energy, when metabolized, glucose also provides the necessary precursors to support the synthesis of proteins, nucleotides, and lipids.

Just as aerobic glycolysis can be a distinguishing attribute of cancer cells, most solid tumors are also characterized by a lipogenic phenotype [6]. While normal cells generally rely on dietary intake to provide an ample supply of fatty acids, cancer cells often require that fatty acids be generated *de novo*, regardless of their exogenous levels [7]. This requirement is critical in order for tumors to maintain proliferation and viability. As a result, the metabolism of fatty acids, in particular their biosynthesis, has gained significant attention in the past decade as a biomarker and therapeutic target in multiple cancers.

As discussed above, the metabolism of glucose provides the precursors for numerous macromolecules, including fatty acids. However, the transition from glucose to fatty acid is a distinctly non-linear process that is coordinated through the action of numerous enzymes localized in various cellular compartments (**Fig. 1**). While most glucose consumed in glycolysis is ultimately metabolized into lactate, some of the pyruvate generated during this reaction will be further metabolized into the fatty acid synthesis pathway. In order to do this, pyruvate is transported into the mitochondria and converted to acetyl-CoA. Since fatty acid synthesis takes place in the cytosol and the mitochondrial membrane is impermeable to acetyl-CoA, it must first be converted into citrate by citrate synthase in the tricarboxylic acid (TCA) pathway. In non-proliferating cells, the TCA cycle generally serves to synthesize ATP from oxidizable substrates,

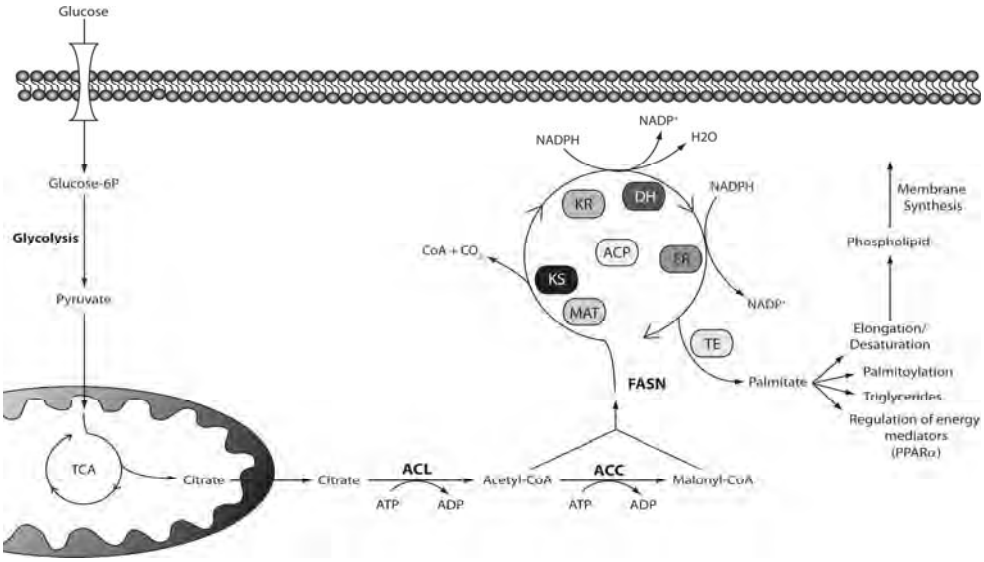

Figure 1. Schematic of the fatty acid synthesis pathway.

such as amino acids. However, in rapidly dividing cells, many of the intermediates, particularly citrate, that are generated during the cycle are effluxed from the pathway in a process termed cataplerosis [2]. Once citrate is shuttled into the cytosol, it is cleaved by ATP-citrate lyase (ACL) into acetyl-CoA and oxaloacetate, comprising the first step of fatty acid synthesis [8]. It is worth noting that the carbons utilized for the production of acetyl-CoA are derived from glucose. Once within the cytosol, acetyl-CoA is converted to malonyl-CoA via carboxylation by acetyl-CoA carboxylase (ACC), the rate-limiting enzyme in the fatty acid synthesis pathway. Finally, fatty acid synthase (FASN) catalyzes the ultimate steps of fatty acid synthesis, yielding the 16-carbon fatty acid palmitate [6].

Fatty acid synthase in tumor cells

FASN is a multifunctional protein, consisting of 7 domains: the malonyl/acetyltransferase (MAT), ketoacyl synthase (KS), β-ketoacyl reductase (KR), β-hydroxyacyl dehydratase (DH), enoyl reductase (ER), acyl carrier protein (ACP), and thioesterase (TE) domains (**Fig. 1**) [9]. In

a series of thirty-two reactions, FASN condenses seven molecules of malonyl-CoA onto an acetyl-CoA head group, using NADPH as a cofactor, to produce the long-chain fatty acid, palmitate [10]. In total, fatty acid synthesis requires seven ATP, one molecule of acetyl-CoA, seven molecules of malonyl-CoA, fourteen NADPH, and 14 hydrogens per molecule of palmitate synthesized. Ultimately, the heavy reliance of cancer cells on glucose metabolism relays into their lipogenic phenotype by providing many of these precursors.

Once palmitate has been generated, it can be utilized for multiple cellular functions (**Fig. 1**). It can be elongated to stearate using malonyl-CoA as a substrate [11]. Palmitate (16:0) and stearate (18:0) can also be desaturated by stearoyl-CoA desaturase 1 (SCD1) to yield palmitoleate (16:1n-9) or oleate (18:1n-9), respectively [12]. These newly synthesized fatty acids are then used to support phospholipid production, and to a significantly lesser extent, triglyceride synthesis. In cancer cells, the majority of *de novo* synthesized fatty acids are specifically enriched into lipid rafts during membrane biogenesis [13]. In this context, it is hypothesized that increased fatty acid synthesis provides the lipid precursors necessary to produce the platforms from which so many intracellular signaling events are initiated.

Aside from membrane biogenesis, FASN can also have an impact on cellular signaling through regulation of protein palmitoylation [14]. For example, FASN activity is required for palmitoylation of Wnt1 and subsequent activation of beta-catenin. A proteomic survey of palmitoylated proteins identified nearly 400 candidates, suggesting that FASN activity could have a wide-ranging influence on protein activity and localization through this post-translational modification [15]. It has also been demonstrated that, at least in hepatocytes, FASN derived lipids act as activating ligand for peroxisome proliferator-activated receptor α (PPARα) [16].

Collectively, these findings illustrate that *de novo* fatty acid synthesis occupies a central role in regulating multiple dynamic processes in tumor cells.

Utilization of positron emission tomography in imaging tumor metabolism: ^{18}F-FDG

Over the past decade, PET-based imaging has revolutionized cancer therapy by non-invasively imaging the aberrant metabolism of tumors to better diagnose and assess early response to therapy. The unique ability of PET to image cell metabolism is derived from a combination of the physical characteristics of positron emitting isotopes, advanced imaging technology, and novel radiochemistry. These factors together with an understanding of exploitable aberrant metabolic pathways in cancer has led to the development of a slew of radiotracers that have the potential to further change the landscape of imaging cancer and response to novel therapies, including small molecule inhibitors of metabolism.

Nuclear-based imaging modalities, including PET, are fundamentally different from traditional diagnostic x-ray imaging, which produce planar and computed tomography (CT) radiographs. Traditional radiographs are anatomic images that differentiate tissues based on their inherent density differences. This is accomplished by passing externally produced x-rays through the body, which are then differentially blocked (attenuated) by distinct tissue densities. The remaining non-attenuated x-rays are captured on the opposite side of the body. Tissues of high density, such as bone, allow few x-rays to pass through, consequently appearing “white” on the processed clinical image (**Fig. 2**). In contrast, tissues such as lungs, which have a very low density, allow ample x-rays to pass through and appear “black” on a processed image. Further distinction between tissues can be gained by the injection of non-targeted high density contrast

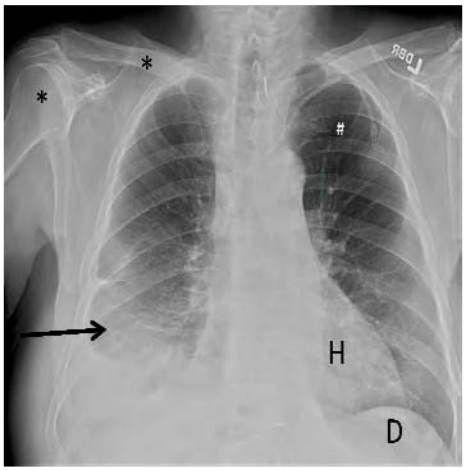

Figure 2. Radiographic imaging of tumor. Chest radiograph of a patient with a right pleural effusion (long arrow). Bone (*) appears white. Low density tissues, such as lung (#), appear darker. Abnormal fluid in the pleural space (pleural effusion) of the right hemithorax appears "whiter" than expected (arrow), indicating a material denser than lung, such as an abnormal fluid collection, is present. (H) heart. (D) diaphragm.

that differentially perfuses to more vascular tissues, such as tumors.

In contrast to traditional radiographs, in nuclear-based imaging physiological amounts of a gamma emitting radioactive compound is injected or ingested by a patient. Each class of clinical tracers has different distribution characteristics based on its chemistry and affinity to normal or diseased tissue. For example, iodine is taken up by functioning thyroid and differentiated thyroid cancer tissue. Therefore, ^{123}I-NaI, a single photon gamma emitter, is routinely utilized in non-physiologic doses to non-invasively detect functioning or malignant thyroid tissue. The distribution of a nuclear tracer is imaged with a traditional gamma camera that provides a functional map of the tracer biodistribution (**Fig. 3**).

While traditional nuclear imaging techniques rely on single photon gamma emitting probes, the sensitivity and resolution of such images are inherently limited by the physics of single photon gamma emitters and imaging systems. In contrast, PET imaging exploits the unique physical characteristics of positron emitting radionuclides, such as ^{18}F and ^{11}C, to provide

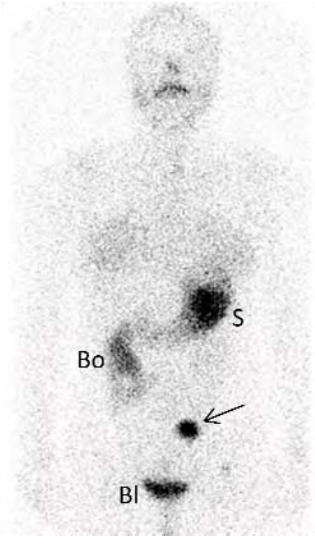

Figure 3. Biodistribution of ^{123}I imaged by a nuclear medicine gamma camera. A patient with a history of thyroid cancer was administered oral ^{123}I-NaI. The tracer distributed physiologically to the stomach (S), bowel (Bo) and bladder (Bl). There is also an abnormal focus of activity (arrow) in the left pelvis that was subsequently confirmed by biopsy to be iodine-avid metastatic thyroid malignancy.

sensitivity and resolution that is orders of magnitude better than traditional single photon nuclear imaging, making it the most sensitive imaging technique currently utilized in the clinic. Positron emitting radionuclides produce characteristic positrons from their nuclei, which travel a short distance of a few millimeters before losing their energy and combining with a nearby electron to trigger an "annihilation" event. This results in the conversion of the positron and electron into *two* gamma rays of exactly 511 keV, emitted 180 degrees from each other. The characteristic energy (511keV) and the angle of emission (180) of the gamma rays are exploited by sophisticated PET scanners that contain a ring of detectors surrounding the patient. These PET scanners only register events that are interpreted as containing the correct energy emission (511 keV) and characteristic simultaneous (coincident) hits on two detectors that are 180 degrees apart. This latter characteristic allows PET "coincident" scanners to precisely detect and localize true events as opposed to scatter or noise, giving it a significantly superior sensitivity and resolution compared to traditional single photon nuclear imaging or MR-based imaging.

Radiotracers utilized in PET imaging generally consist of radionuclei with a short half-life, such as ^{18}F, ^{11}C, ^{13}N, and ^{15}O, integrated into substrates utilized in metabolic pathways that are aberrant in tumor cells. For example, because tumors are so often characterized by altered glucose metabolism, ^{18}F-fluorodeoxyglucose (FDG)-PET has been particularly effective in characterizing malignancies that have a glycolytic phenotype. FDG, a glucose analog, is actively transported into cells in proportion to their metabolic activity where it is phosphorylated but unable to be further metabolized or exported [17-18]. Because many tumors display unfettered growth and high energy demands, they are often classified as FDG avid. Consequently, malignant foci of high positron accumulation stand out on a background of normal physiological signal (**Fig. 4**). A number of cancers, including, but not limited to, non-small cell lung cancer, certain lymphomas, melanoma, and head and neck cancer are all FDG avid malignancies, and their evaluation is well served by FDG-PET [19-22].

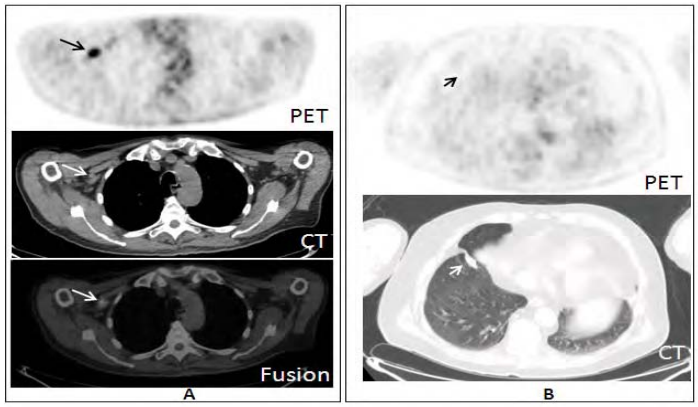

Figure 4. **FDG-PET/CT in malignancy.** (A) In a patient with confirmed lymphoma, a hypermetabolic lymph node takes up excess FDG which is characteristic of malignancy (Upper panel; arrow). A CT image of the same lymph node (middle panel; arrow) would not meet size criteria for malignancy. (B) FDG-PET and CT in a patient with a lung nodule (arrow) to evaluate for hypermetabolism characteristic of malignancy. No FDG uptake is seen in this lung nodule (upper panel), indicating that it is likely benign in nature. Yearly follow-up CT images (not shown) demonstrated no growth for two years after the PET/CT, confirming the benign nature of the nodule.

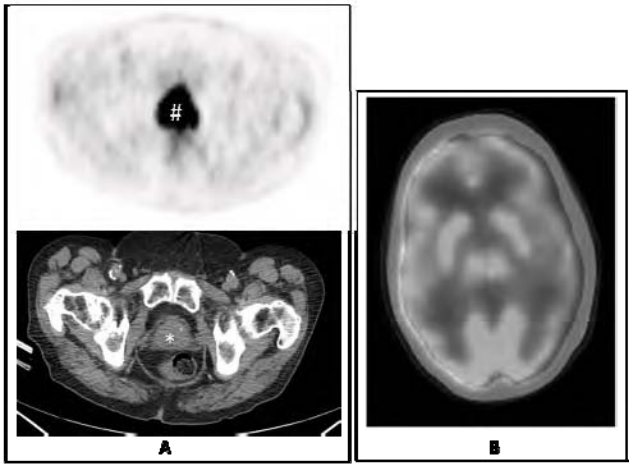

Figure 5. FDG-PET is not effective in imaging certain tumor types. (A) An FDG-PET/CT demonstrates a large amount of tracer on the PET component (#) localizing to the prostate (*) on the CT component. This signal is not from the prostate but is emanating from the inferior portion of the bladder, which is filled with excreted FDG in the urine. (B) A brain FDG-PET/CT of a patient with metastatic melanoma. Image demonstrates characteristically high FDG uptake by normal brain cells, consequently masking multiple brain metastasis.

There are, however, a variety of other cancers, including primary hepatocellular carcinomas, renal cell carcinomas, and certain types of lymphoma, that are not easily visualized by ^{18}F-FDG PET [23-25]. ^{18}F-FDG PET is particularly ineffective in prostate cancer [26-27]. This is mainly because primary prostate tumors are generally not highly glycolytic, and thus do not readily accumulate FDG. Consequently, FDG uptake is no greater in prostate tumors than in benign prostatic hyperplasia (BPH) or normal glandular tissue [28-29]. It is important to note that contrary to primary disease, neuroendocrine differentiated and metastatic prostate cancers can be visualized by FDG-PET [28, 30]. Visualization of primary prostate cancer can also be occluded from detection by ^{18}F-FDG PET due to the anatomical proximity of the prostate gland to the bladder (**Fig. 5A**) [27]. Even when bladder emptying is carried out to clear residual isotope prior to imaging, urinary excretion of FDG generally prevents prostate lesions from being detected. Because the brain consumes significant levels of glucose to support normal

function, brain tumors can also become obscured due to high signal in surrounding, non-malignant regions (**Fig. 5B**) [31].

Using ^{11}C-acetate PET to image tumor metabolism

In instances where ^{18}F-FDG may be an inappropriate radiotracer, ^{11}C-acetate is a radiopharmaceutical that holds much promise. Specifically, ^{11}C-acetate could have significant value for the imaging of lipogenic tumors. ^{11}C-acetate is believed to be actively taken into the cell by proton-coupled monocarboxylate transporter [32]. In normal cells, acetate is metabolized in the TCA cycle yielding CO_2 and water [33]. However, in cancer cells, acetate is preferentially utilized for fatty acid synthesis as a component of acetyl-CoA. Upon entry into the cell, acetate is converted to acetyl-CoA by acetyl-CoA synthase (ACeS), thereby making it available to feed into the fatty acid synthesis pathway. ACeS is found in two isoforms (ACeS1 and ACeS2), which are present in the cytoplasm and mitochondria, respectively. Interestingly, non-glycolytic tumor cells that exhibit low ^{18}F-FDG uptake can express high levels of ACeS and have correspondingly high ^{11}C-acetate uptake [34-35]. The knockdown of ACeS 1 and 2 with siRNA not only reduces uptake of ^{11}C-acetate into tumor cells, it also decreases overall cell viability, suggesting an important role for this enzyme in tumor cells [34]. Because acetate was thought to only be available during a limited set of circumstances, it is currently unclear what role or to what extent physiological levels of acetate play in *de novo* fatty acid synthesis. However, in recent years it has become apparent that acetate can be made available from histone and non-histone protein de-acetylation by sirtuins, providing potential substrate for ACeS 1 and 2 to shuttle acetate into the fatty acid synthesis pathway [36]. It is worth noting that inactivation of ACeS by acetylation results in decreased incorporation of ^{14}C-acetate into lipids [36].

Combined, these data suggest that ACeS may play a role in tumor lipid metabolism and ^{11}C-acetate uptake by tumors.

The potential utility of ^{11}C-acetate PET in tumors contrasts with its original clinical application, which was to assess myocardial function [37]. In myocardial tissues, carbons derived from ^{11}C-acetate are incorporated into CO_2 during the TCA cycle, allowing for PET visualization of oxygen consumption. However, as previously mentioned, ^{11}C-acetate preferentially partitions into lipids in cancer cells. The majority of studies analyzing the efficacy of ^{11}C-acetate PET in tumors have focused on the detection of prostate cancer [38-42]. As mentioned, primary prostate cancer is a particularly poor candidate for standard ^{18}F-FDG PET imaging due to its lower metabolic rate and proximity to the bladder. One of the most common courses of treatment for prostate cancer patients is hormone therapy or androgen ablation. However, prostate tumors frequently become unresponsive to androgen therapy due to a number of factors, including upregulation of androgen receptors, emerging as castration-refractory prostate cancers (CRPC) [43-44]. In order to assess the effectiveness of treatment, serum prostate specific androgen (PSA) levels are often monitored. Studies have shown that PSA levels greater than 2ng/ml in patients who had received radical prostatectomy as well as salvage radiotherapy increase the likelihood of disease relapse by at least two-fold [45]. However, PSA levels do not always increase in the instance of tumor recurrence. Sandblom et al demonstrated that recurrent prostate lesions in patients exhibiting PSA levels as low as 0.5 ng/ml could still imaged using ^{11}C-acetate PET [39].

In addition to PSA levels, therapy validation is also monitored by assessing total prostate volume using conventional imaging techniques, such as CT and MRI [46-47]. However, in some cases, CT and MRI have been shown to have limitations in detecting recurrent prostate lesions

[40, 48]. Furthermore, assessment of therapy success can take up to three months using such techniques. Conversely, ^{11}C-acetete PET detected metabolic changes within days of androgen ablation in a murine model of prostate cancer [46]. Furthermore, in human studies, ^{11}C-acetate PET has been shown to be effective at detecting prostate tumors, not only in the prostate bed, but also in lung, lymph node, and bone metastases [40-41]. These findings are especially significant since CT and MRI often fail to detect lymph node metastases that are smaller than 1 cm in diameter [40].

In terms of correlations between ^{11}C-acetate incorporation in prostate cancer cells and fatty acid synthesis, it is important to note that increased FASN expression is tightly associated with prostate cancer. Expression of FASN has been linked to poor prognosis, risk of disease recurrence, and the stage of the cancer [49-51]. Coincident with these facts, the uptake of ^{11}C-acetate in prostate cancer correlates with FASN expression and is abrogated by treatment with a small molecule inhibitor of FASN [52]. Together, these data demonstrate that tumors can be monitored by ^{11}C-acetate PET as a function of their lipogenic phenotype; specifically, the *de novo* fatty acid synthesis pathway.

In addition to prostate cancer, there are a number of other tumors in which ^{11}C-acetate PET has demonstrated success, including hepatocellular carcinoma (HCC), thymomas, renal cancers, and bronchioloalveolar carcinoma [23, 53-55]. In HCC, ^{18}F-FDG has proven inconsistent in its ability to detect liver masses. This is due in part to normal glucose utilization and variations in the activity of certain enzymes, such as glucose-6-phosphatase, in hepatic lesions [56]. On the other hand, ^{11}C-acetate PET was significantly more effective at detecting hepatic lesions than ^{18}F-FDG (87.3% versus 47.3%) in a cohort of patients with various categories of liver masses, including HCC, as well as hepatic metastasis arising from peripheral

sites [23]. Thymic tumors are also difficult to detect by ^{18}F-FDG due to their relatively low rate of growth and glucose uptake. While thymomas generally show limited sensitivity to ^{18}F-FDG, several studies have reported that tumors arising from thymic tissue can be positively imaged using ^{11}C-acetate [53, 57]. Importantly, FASN expression has been shown to be significantly increased in cancers that can be imaged with ^{11}C-acetate PET [58-59]. Collectively, these studies demonstrate the utility of ^{11}C-acetate PET in exploiting the lipogenic phenotype of cancer cells to detect certain tumors.

Using ^{11}C-acetate PET to predict response to therapies that *directly* target the fatty acid synthesis pathway

In addition to using new modalities to diagnose or monitor tumors, it is intriguing to speculate that ^{11}C-acetete PET may also be used to monitor specific cancer therapies. With the advent and expansion of targeted therapy, it is now possible to administer therapeutic agents with reduced or minor effects on normal tissue. However, it remains important to validate that the "magic bullet" homed in on its intended target. Aside from tumor regression, there are often few options to monitor therapy in the near term or real time. However, PET/CT provides a superb opportunity for scrutinizing certain targeted therapies, both directly and indirectly. The archetypal radiotracer, FDG, is the most commonly used agent in this regard. There is no more striking an example as with imatinib mesylate, a c-kit inhibitor, used to treat gastrointestinal stromal tumors (GIST). Imatinib has been demonstrated to dampen glucose transporter recruitment to the plasma membrane and thus rapidly reduce tumor ^{18}F-FDG uptake [60]. Early clinical studies investigating the efficacy of imatinib in treating GIST revealed remarkable shifts in avidity to FDG after only 1-7 days of therapy. In terms of its prognostic abilities, a favorable response to imatinib predicted longer progression-free survival (92% vs. 12%), whereas lack of

response correlated with disease progression and poor survival [61]. A study by Engelman et al demonstrated that FDG uptake was also a determinant of whether tumors respond appropriately to a dual PI3-kinase/mTor inhibitor known as NVP-BEZ235 [62]. These studies clearly establish that the application of PET/CT may well prove to be proactive in guiding early treatment decisions.

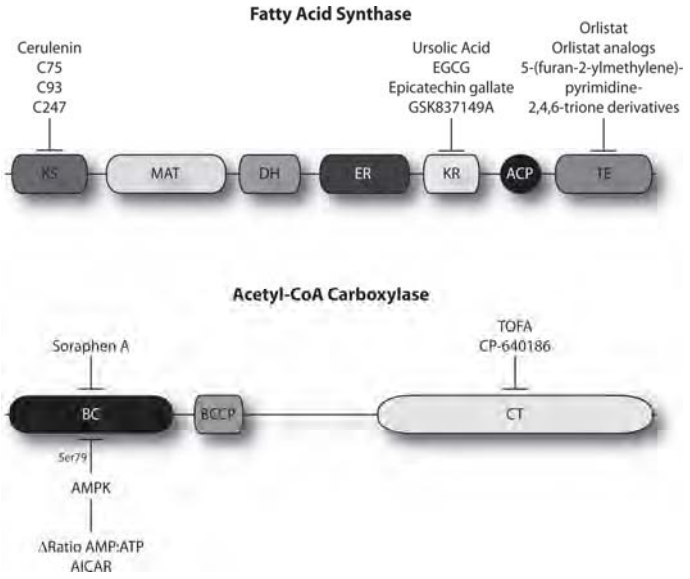

Figure 6. Inhibitors directed against select domains of FASN and ACC. Small molecule inhibitors that target the KS, KR and TE domains have been described. Small molecule inhibitors of the BC and CT domain of ACC have also been described. ACC can also be inhibited by phosphorylation at Ser 79 in the BC domain.

Based on the demonstration that ^{11}C-acetate is equivalent to, or can outperform FDG in diagnosis, staging, and predicting disease progression in certain cancers, it is logical that ^{11}C-acetate could also be used to stratify patients for specific therapies, as well as a method to monitor response to therapy. Furthermore, because ^{11}C-acetate PET can be used to directly monitor FASN activity, there is potential that this approach may be an effective means to validate FASN inhibitors as they progress into and through clinical development. Significant effort has been directed towards the discovery and development of agents that can inhibit the activity of FASN. That FASN comprises seven functional domains and six enzymatic pockets provides ample opportunity to target multiple functions within the single protein. Accordingly, a number of inhibitors with specificity toward the different domains of FASN have been identified (**Fig. 6**). The first recognized small molecules with FASN inhibitory activity targeted the

ketoacyl synthase (KS) domain of FASN. The KS domain coordinates with the activity of the MAT domain to catalyze the formation of an acetoacetyl-ACP intermediate, which then serves as a substrate for elongation by three of the other domains of FASN (KR, DH, and ER domains). Cerulenin, a naturally occurring antifungal derived from *Cephalosporium caerulens*, rapidly and irreversibly inhibits the initiation of fatty acid synthesis by binding the KS domain, thereby inducing death in tumor cells [63-64]. Synthetic analogs of cerulenin, including C75, C93, and C247, have also demonstrated strong anti-tumor activity [65-67].

In addition to the KS domain, the TE domain of FASN has also proven to be a viable drug target. Once palmitate is generated through the enzymatic activity of the KS, MAT, KR, DH, and ER domains of FASN, the TE domain is responsible for hydrolyzing the final 16-carbon product from the enzyme. The first TE inhibitor to be indentified was orlistat, an FDA-approved anti-obesity drug [68]. Orlistat binds the TE domain through covalent interaction with serine 2308, the catalytic serine in the TE active site [69]. Since the discovery of orlistat as a FASN inhibitor, a number of orlistat analogs have been developed that also target the FASN-TE domain. These newly synthesized analogs share with orlistat a beta-lactone moiety as the distinguishing chemotype [70]. Beta-lactam derivatives of orlistat have also been described [71]. Altogether, several compounds similar to orlistat have been identified that exhibit improved FASN inhibitory activity, solubility, and tumor cells selectivity. Following the identification of orlistat, a subsequent high-throughput screen identified 5-(furan-2-ylmethylene) pyrimidine-2,4,6-trione as a novel pharmacophore capable of inhibiting FASN-TE with sub-micromolar Ki's. Importantly, these compounds demonstrated selectivity against breast tumor cells when compared to immortalized breast epithelial cells [72].

Finally, the KR domain of FASN has been the focus of intense therapeutic targeting. Ursolic acid, a pentacyclic triterpenoid acid, as well as the tea polyphenols, epigallocatechin gallate (EGCG) and epicatechin gallate, interact with the KR domain of FASN, thereby inhibiting its activity [73-74]. Recently, GSK837149A was also serendipitously identified as a potent and selective inhibitor of the KR domain [75]. Unfortunately, this compound and subsequent analogs exhibit poor cellular permeability.

In order to assist in the development and design of novel FASN inhibitors, a substantial effort has been placed on advancing the knowledge base concerning the structure of FASN. There are two high-resolution structures of the human FASN-TE domain, including one with orlistat bound in the active site [69, 76]. Recently, the structure of the beta-ketoacyl synthase (KS) domain linked to the malonyl/acetyltransferase (MAT) domain of human FASN was also reported [77]. Given that such structures provide significant insight into the geometry of the substrate-binding site, they should greatly enhance structure-based design of novel FASN inhibitors. Having lead compounds identified in orlistat and cerulenin, subsequent structure-activity relationship (SAR) analysis from follow-up studies, and the identification of new pharmacophores from activity-based screening, greatly enhances the potential of translating FASN inhibitors into the clinic.

Although there are currently no small molecule inhibitors directed against FASN in the clinic, the likelihood of such molecules being developed is imminent. At such time, it would be beneficial to have in hand a procedure to monitor the efficacy of such inhibitors quickly and effectively. Because ^{11}C-acetate uptake directly correlates with FASN levels in prostate cancer, ^{11}C-acetate PET may predict which patients would respond best to FASN inhibitors in a clinical setting and determine whether the pathway is blocked following their administration. This

hypothesis was supported by findings demonstrating that that the FASN inhibitor C75 could reduce ^{11}C-acetate SUV by up to 60% in prostate cancer xenografts [52]. It is worth noting that inhibition of FASN activity also reduces the uptake of FDG in an orthotopic model of lung cancer [78].

In addition to fatty acid synthase, a number of other enzymes in the fatty acid synthesis pathway are also commonly overexpressed in cancer. For example, protein expression of ACC, the rate-limiting enzyme upstream of FASN, has been shown to be upregulated in numerous tumor types, including prostate cancer, hepatocellular carcinoma, and breast cancer [79-81]. Importantly, immunohistochemical analysis of breast tissue from patients with or without cancer demonstrated that the overexpression of ACC did not simply occur once a patient had progressed to a more advanced or malignant disease phenotype, but could be detected in the earliest stages of cancer development, including ductal carcinoma *in situ* (DCIS) and lobular carcinoma *in situ* (LCIS) [82]. As a result, ACC is believed to be an excellent candidate for targeted cancer therapy. Currently, several drugs that block the activity of ACC exist. From 2007 to 2008, approximately 18 distinct patents were published regarding the development of inhibitors directed against ACC [83]. One of the earliest ACC inhibitors to be identified was TOFA (5-tetradecyloxy-2-furoic acid), a lipophilic fatty acid mimetic that targets the carboxyltransferase (CT) activity of ACC (**Fig. 6**) [84-85]. TOFA has proven to be cytotoxic to a variety of different cancer types, including breast, lung, and colon carcinomas [85-86]. In terms of ^{11}C-acetate accumulation, treatment of several prostate cancer lines with TOFA significantly blocked the uptake of this radiotracer [52]. Additional inhibitors of ACC include Soraphen A and CP-640186 that inhibit the BC and CT domains of the enzyme, respectively [87-88]. Although ACC inhibitors have anti-tumor potential, all ACC inhibitors that have been described thus far are not

isoenzyme selective. While ACC1 is the enzyme responsible for generating malonyl-CoA for fatty acid synthesis, it is very closely related to ACC2, the mitochondrial isoenzyme that produces malonyl-CoA to regulate β-oxidation [89-90]. Importantly, none of the inhibitors have been analyzed *in vivo* for their anti-tumor activity or ability to inhibit tumor fatty acid synthesis.

In addition to inhibiting ACC with small molecules, the activity of this enzyme can also be abrogated following phosphorylation by PKA and AMP-activated kinase (AMPK). Phosphorylation by these serine/threonine kinases renders ACC inactive, effectively shutting down fatty acid synthesis [91]. Importantly, AMP mimetics, like AICAR (5-aminoimidazole-4-carboxamide-1-β-4-ribofuranoside), have demonstrated the potential to activate AMPK, subsequently inactivating ACC [92]. Moreover, these compounds can inhibit proliferation and induce cell death in tumor cells, including those of the prostate. There is also epidemiological evidence demonstrating that the anti-diabetic drug metformin, which works through an AMPK-dependent mechanism, decreases the risk of prostate cancer [93]. Given that acetate incorporation into tumor cells has been found to directly correlate with the extent of fatty acid synthesis, the efficacy of treatment with molecules that regulate the activity of ACC could easily be monitored using ^{11}C-acetate PET.

Using ^{11}C-acetate PET to predict response to therapies that *indirectly* target the fatty acid synthesis pathway

The same pathways that are important for initiating and driving the development and progression of cancer also have primary roles in regulating the expression of enzymes in the fatty acid synthesis pathway (**Fig. 7**). As a result, there is potential that the fatty acid synthesis pathway, monitored by ^{11}C-acetate PET/CT, could serve as a surrogate marker for validating the

efficacy of or monitoring response to a myriad of therapeutic agents. Support for this idea was provided by an analysis of the response of renal cell carcinoma to sunitinib, a multi-targeted receptor tyrosine kinase inhibitor that blocks platelet derived growth factor (PDGF) and vascular endothelial growth factor (VEFG) receptors. In one case, remission was predicted by ^{11}C-acetate PET after only two weeks of treatment [94]. Of note**,** gene expression for key enzymes involved in lipid synthesis, specifically FASN, can be elevated by PDGF [95]. While this study did not correlate the decrease in ^{11}C-acetate with changes in FASN expression, it is tempting to

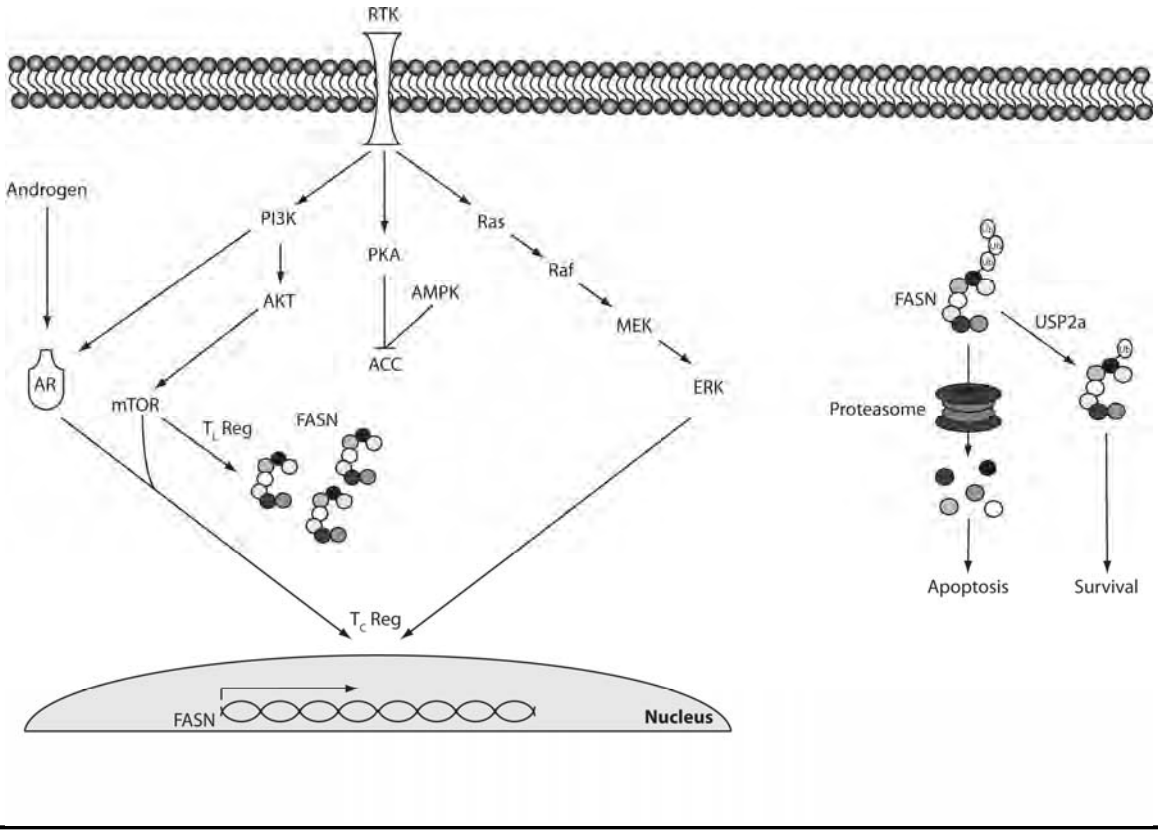

Figure 7. Schematic of FASN regulation at the transcriptional, translational, and post-translational level. Receptor tyrosine kinase (RTK) signaling can lead to the induction of the PI3K/AKT, PKA, and Ras/MAPK pathways. Aberrant signaling through these pathways leads to the overexpression of FASN due to transcriptional (T_C) or translational regulation (T_L). Androgen binding to the androgen receptor (AR) increased FASN expression. De-ubiquitination stabilizes FASN protein levels to promote cellular survival.

speculate that the two are linked.

There are a number of other oncogenic pathways that augment FASN expression and are targets for therapeutic development. One of the primary drivers of FASN expression is the PI3-kinase/Akt axis. Blockade of PI3-kinase (PI3K) activity and Akt expression leads to reduced FASN protein expression in cell lines from multiple tumors, including prostate, breast, and ovarian [81, 96-97]. Similarly, FASN expression correlates with loss of Pten and poor outcome in patients with prostate cancer [50, 96-97]. Currently, there are over twenty ongoing clinical trials evaluating the safety and/or efficacy of PI3K inhibitors in cancer patients (clinicaltrials.gov). Importantly, many of these compounds, including the pan PI3K inhibitors SF1126 and PX-866, have been found to target solid tumors that are particularly well served by ^{11}C-acetate PET imaging, namely prostate cancer and renal cell carcinoma [98-99]. Consequently, it stands to reason that ^{11}C-acetate PET analysis of patients receiving such inhibitors may be effectively used to monitor the value of treatment. Like PI3K activity, expression of H-Ras can also lead to transcriptional induction of FASN expression (**Fig. 7**) [100]. The efficacy of numerous MAPK inhibitors, a downstream target of the Ras signaling pathway, are also currently in clinical trials (clinicaltrials.gov).

Although FASN overexpression is primarily regulated at the transcriptional level, there are complimentary mechanisms that can also contribute to increased expression. For example, in prostate cancer, the *FASN* gene is frequently duplicated in a manner that correlates with increased protein expression [101]. FASN levels can also be increased at the translational level through the activation of the 5'- and 3'-UTRs of its mRNA following mTor signaling (**Fig. 7**) [81]. Lastly, the FASN protein can be stabilized by the deubiquitinating enzyme, ubiquitin-

specific protease-2a (USP2a), which can prevent the proteasome-mediated turnover of FASN, thereby increasing protein levels [102].

In addition to the oncogenic pathways and mechanisms mentioned above, FASN expression can also be driven by variations in hormone levels, such as androgen, in hormone sensitive tissues, including the prostate and breast [103-104]. Consequently, treatment of androgen-responsive prostate tumor lines with dutasteride (a 5-alpha-reductase inhibitor that blocks the conversion of testosterone to dihydrotestosterone) significantly decreases FASN protein levels [105]. As discussed earlier, the use of ^{11}C-acetete PET has proven effective in monitoring the response to androgen ablation, suggesting that this modality can also be used to monitor response to other therapies or relapse in men receiving hormone ablation therapy [46]. Moreover, it may detect resistance or relapse to hormone therapy earlier than PSA recurrence post nadir. Collectively, these studies suggest that PET analysis of ^{11}C-acetate uptake could effectively monitor response to therapies that indirectly affect FASN expression and activity, likely within a shorter time frame than monitoring tumor regression.

Potential limitations of ^{11}C-acetate PET

While ^{11}C-acetate PET has demonstrated promise in the diagnosis and staging of several cancers, as well as in monitoring fatty acid synthesis, there are some limitations to its wide spread implementation. One hurdle is the half-life of the ^{11}C isotope. With a half-life of 20 minutes, the use of ^{11}C-acetate to image tumors and monitor fatty acid synthesis would be limited to institutions with in-house cyclotrons. A potential solution to effectively monitor fatty acid synthesis with acetate in instances where ^{11}C-acetate is not feasible could be the use of 2-^{18}F-fluoroacetate [106].

Although the uptake of ^{11}C-acetate has been directly associated with FASN expression and activity, there are biological caveats to the use of acetate-PET/CT. One is that acetate, in addition to serving as a precursor for fatty acid synthesis, is also used for other reactions within a cell. Specifically, acetate is used for protein acetylation, especially for histones [107]. Additionally, acetate is utilized in cholesterol synthesis, which has been linked by epidemiology and experimental evidence to prostate cancer [108]. As a result, it is possible that ^{11}C-acetate could have utility directly related to fatty acid synthesis in some cancers, while being associated with additional pathways in other cancers.

Conclusions

Significant progress has been made in deciphering the metabolic alterations that occur in cancer cells and how these changes might be exploited for the development of novel anti-cancer drugs. However, an effective means to validate the efficacy of such therapies in the clinical setting remains a high priority [109]. To date, therapy validation has centered on morphological parameters, namely tumor size, as defined by the Response Evaluation Criteria in Solid Tumors (RECIST) guidelines [21]. While the overarching goal of cancer therapy is to eradicate the patient's tumor burden, primarily focusing on tumor size is not always an ideal means to monitor therapy success since extended periods of time may be required before such changes are observed. Furthermore, in certain cancers, particularly that of the prostate, quantification of tumor mass is a difficult task, nullifying a proper determination as to drug efficacy according to RECIST standards [110]. Finally, merely assessing reduction in tumor size does not discriminate whether the drug of interest is specifically inhibiting the intended target.

Employing PET technology provides value beyond evaluation of tumor load for a number of reasons. First, PET is non-invasive. Second, it allows for repetitive imagining within short time frames. More specific to the current topic, PET imaging provides a means to monitor the effects of specific therapies on a given metabolic pathway often dysregulated in cancer cells, including glucose uptake and fatty acid synthesis. The goal of this review was to demonstrate the correlation between ^{11}C-acetate uptake in tumor cells and the expression/activity of proteins involved in the fatty acid synthesis pathway in various cancers. Based on this correlation, we propose that ^{11}C-acetate PET will have utility beyond diagnosis of specific cancers. ^{11}C-acetate PET could be informative about patient stratification for therapy, response to specific therapeutics, and treatment decisions following surgical removal of tumors. Specifically, the development of FASN and ACC inhibitors and their subsequent translation into the clinic will require validation that could be provided by ^{11}C-acetate PET. In addition, we have provided evidence suggesting that therapeutic interventions that indirectly impact the fatty acid synthesis pathway could also be monitored by ^{11}C-acetate PET. Overall, the ubiquitous requirement for *de novo* fatty acid synthesis in cancer cells provides an opportunity to harness this trait with modern PET technology in order to provide better outcome for patients afflicted with certain cancers.

Conflict of Interest: The authors declare no conflict of interest.

Acknowledgements: Research support from NIH/NCI CA114104 and the Department of Defense Prostate Cancer Research ProgramW81XWH-09-1-0204 to SJK.

References

1. Dunphy, M. P., and Lewis, J. S. Radiopharmaceuticals in preclinical and clinical development for monitoring of therapy with PET. *J Nucl Med*, **2009,** 50 Suppl 1(106S-121S.
2. DeBerardinis, R. J., Lum, J. J., Hatzivassiliou, G., and Thompson, C. B. The biology of cancer: metabolic reprogramming fuels cell growth and proliferation. *Cell Metab*, **2008,** 7(1), 11-20.
3. Warburg, O. On respiratory impairment in cancer cells. *Science*, **1956,** 124(3215), 269-270.
4. Kim, J. W., and Dang, C. V. Cancer's molecular sweet tooth and the Warburg effect. *Cancer Res*, **2006,** 66(18), 8927-8930.
5. Gatenby, R. A., and Gillies, R. J. Why do cancers have high aerobic glycolysis? *Nat Rev Cancer*, **2004,** 4(11), 891-899.
6. Swinnen, J. V., Brusselmans, K., and Verhoeven, G. Increased lipogenesis in cancer cells: new players, novel targets. *Curr Opin Clin Nutr Metab Care*, **2006,** 9(4), 358-365.
7. Ookhtens, M., Kannan, R., Lyon, I., and Baker, N. Liver and adipose tissue contributions to newly formed fatty acids in an ascites tumor. *Am J Physiol*, **1984,** 247(1 Pt 2), R146-153.
8. Hatzivassiliou, G., Zhao, F., Bauer, D. E., Andreadis, C., Shaw, A. N., Dhanak, D., Hingorani, S. R., Tuveson, D. A., and Thompson, C. B. ATP citrate lyase inhibition can suppress tumor cell growth. *Cancer Cell*, **2005,** 8(4), 311-321.
9. Smith, S., Witkowski, A., and Joshi, A. K. Structural and functional organization of the animal fatty acid synthase. *Prog Lipid Res*, **2003,** 42(4), 289-317.
10. Chirala, S. S., and Wakil, S. J. Structure and function of animal fatty acid synthase. *Lipids*, **2004,** 39(11), 1045-1053.
11. Cinti, D. L., Cook, L., Nagi, M. N., and Suneja, S. K. The fatty acid chain elongation system of mammalian endoplasmic reticulum. *Prog Lipid Res*, **1992,** 31(1), 1-51.
12. Enoch, H. G., Catala, A., and Strittmatter, P. Mechanism of rat liver microsomal stearyl-CoA desaturase. Studies of the substrate specificity, enzyme-substrate interactions, and the function of lipid. *J Biol Chem*, **1976,** 251(16), 5095-5103.
13. Swinnen, J. V., Van Veldhoven, P. P., Timmermans, L., De Schrijver, E., Brusselmans, K., Vanderhoydonc, F., Van de Sande, T., Heemers, H., Heyns, W., and Verhoeven, G. Fatty acid synthase drives the synthesis of phospholipids partitioning into detergent-resistant membrane microdomains. *Biochem Biophys Res Commun*, **2003,** 302(4), 898-903.
14. Fiorentino, M., Zadra, G., Palescandolo, E., Fedele, G., Bailey, D., Fiore, C., Nguyen, P. L., Migita, T., Zamponi, R., Di Vizio, D., Priolo, C., Sharma, C., Xie, W., Hemler, M. E., Mucci, L., Giovannucci, E., Finn, S., and Loda, M. Overexpression of fatty acid synthase is associated with palmitoylation of Wnt1 and cytoplasmic stabilization of beta-catenin in prostate cancer. *Lab Invest*, **2008,** 88(12), 1340-1348.
15. Yang, W., Di Vizio, D., Kirchner, M., Steen, H., and Freeman, M. R. Proteome scale characterization of human S-acylated proteins in lipid raft-enriched and non-raft membranes. *Mol Cell Proteomics*, **2010,** 9(1), 54-70.
16. Chakravarthy, M. V., Pan, Z., Zhu, Y., Tordjman, K., Schneider, J. G., Coleman, T., Turk, J., and Semenkovich, C. F. "New" hepatic fat activates PPARalpha to maintain glucose, lipid, and cholesterol homeostasis. *Cell Metab*, **2005,** 1(5), 309-322.
17. Krohn, K. A., Mankoff, D. A., Muzi, M., Link, J. M., and Spence, A. M. True tracers: comparing FDG with glucose and FLT with thymidine. *Nucl Med Biol*, **2005,** 32(7), 663-671.
18. Sokoloff, L., Reivich, M., Kennedy, C., Des Rosiers, M. H., Patlak, C. S., Pettigrew, K. D., Sakurada, O., and Shinohara, M. The [14C]deoxyglucose method for the measurement of local cerebral glucose utilization: theory, procedure, and normal values in the conscious and anesthetized albino rat. *J Neurochem*, **1977,** 28(5), 897-916.

19. Kim, Y. S., Lee, M. K., Kim, S. J., Kim, I. J., Kim, Y. K., Jo, W. S., and Park, S. K. Prognostic stratification using F-18 FDG PET/CT in patients with advanced stage (Stage III and IV) non-small cell lung cancer. *Neoplasma*, **2010,** 57(3), 241-246.
20. Weiler-Sagie, M., Bushelev, O., Epelbaum, R., Dann, E. J., Haim, N., Avivi, I., Ben-Barak, A., Ben-Arie, Y., Bar-Shalom, R., and Israel, O. (18)F-FDG avidity in lymphoma readdressed: a study of 766 patients. *J Nucl Med*, **2010,** 51(1), 25-30.
21. Bastiaannet, E., Wobbes, T., Hoekstra, O. S., van der Jagt, E. J., Brouwers, A. H., Koelemij, R., de Klerk, J. M., Oyen, W. J., Meijer, S., and Hoekstra, H. J. Prospective comparison of [18F]fluorodeoxyglucose positron emission tomography and computed tomography in patients with melanoma with palpable lymph node metastases: diagnostic accuracy and impact on treatment. *J Clin Oncol*, **2009,** 27(28), 4774-4780.
22. Lonneux, M., Hamoir, M., Reychler, H., Maingon, P., Duvillard, C., Calais, G., Bridji, B., Digue, L., Toubeau, M., and Gregoire, V. Positron emission tomography with [18F]fluorodeoxyglucose improves staging and patient management in patients with head and neck squamous cell carcinoma: a multicenter prospective study. *J Clin Oncol*, **2010,** 28(7), 1190-1195.
23. Ho, C. L., Yu, S. C., and Yeung, D. W. 11C-acetate PET imaging in hepatocellular carcinoma and other liver masses. *J Nucl Med*, **2003,** 44(2), 213-221.
24. Kang, D. E., White, R. L., Jr., Zuger, J. H., Sasser, H. C., and Teigland, C. M. Clinical use of fluorodeoxyglucose F 18 positron emission tomography for detection of renal cell carcinoma. *J Urol*, **2004,** 171(5), 1806-1809.
25. Najjar, F., Hustinx, R., Jerusalem, G., Fillet, G., and Rigo, P. Positron emission tomography (PET) for staging low-grade non-Hodgkin's lymphomas (NHL). *Cancer Biother Radiopharm*, **2001,** 16(4), 297-304.
26. Sung, J., Espiritu, J. I., Segall, G. M., and Terris, M. K. Fluorodeoxyglucose positron emission tomography studies in the diagnosis and staging of clinically advanced prostate cancer. *BJU Int*, **2003,** 92(1), 24-27.
27. Liu, I. J., Zafar, M. B., Lai, Y. H., Segall, G. M., and Terris, M. K. Fluorodeoxyglucose positron emission tomography studies in diagnosis and staging of clinically organ-confined prostate cancer. *Urology*, **2001,** 57(1), 108-111.
28. Jadvar, H., Pinski, J. K., and Conti, P. S. FDG PET in suspected recurrent and metastatic prostate cancer. *Oncol Rep*, **2003,** 10(5), 1485-1488.
29. Effert, P. J., Bares, R., Handt, S., Wolff, J. M., Bull, U., and Jakse, G. Metabolic imaging of untreated prostate cancer by positron emission tomography with 18fluorine-labeled deoxyglucose. *J Urol*, **1996,** 155(3), 994-998.
30. Liu, Y. FDG PET-CT demonstration of metastatic neuroendocrine tumor of prostate. *World J Surg Oncol*, **2008,** 6(64.
31. Olivero, W. C., Dulebohn, S. C., and Lister, J. R. The use of PET in evaluating patients with primary brain tumours: is it useful? *J Neurol Neurosurg Psychiatry*, **1995,** 58(2), 250-252.
32. Waniewski, R. A., and Martin, D. L. Preferential utilization of acetate by astrocytes is attributable to transport. *J Neurosci*, **1998,** 18(14), 5225-5233.
33. Landau, B. R. Acetate's metabolism, CO2 production, and the TCA cycle. *Am J Clin Nutr*, **1991,** 53(4), 981-982.
34. Yun, M., Bang, S. H., Kim, J. W., Park, J. Y., Kim, K. S., and Lee, J. D. The importance of acetyl coenzyme A synthetase for 11C-acetate uptake and cell survival in hepatocellular carcinoma. *J Nucl Med*, **2009,** 50(8), 1222-1228.
35. Yoshii, Y., Waki, A., Furukawa, T., Kiyono, Y., Mori, T., Yoshii, H., Kudo, T., Okazawa, H., Welch, M. J., and Fujibayashi, Y. Tumor uptake of radiolabeled acetate reflects the expression of

cytosolic acetyl-CoA synthetase: implications for the mechanism of acetate PET. *Nucl Med Biol*, **2009,** 36(7), 771-777.

36. Hallows, W. C., Lee, S., and Denu, J. M. Sirtuins deacetylate and activate mammalian acetyl-CoA synthetases. *Proc Natl Acad Sci U S A*, **2006,** 103(27), 10230-10235.
37. Brown, M., Marshall, D. R., Sobel, B. E., and Bergmann, S. R. Delineation of myocardial oxygen utilization with carbon-11-labeled acetate. *Circulation*, **1987,** 76(3), 687-696.
38. Fricke, E., Machtens, S., Hofmann, M., van den Hoff, J., Bergh, S., Brunkhorst, T., Meyer, G. J., Karstens, J. H., Knapp, W. H., and Boerner, A. R. Positron emission tomography with 11C-acetate and 18F-FDG in prostate cancer patients. *Eur J Nucl Med Mol Imaging*, **2003,** 30(4), 607-611.
39. Sandblom, G., Sorensen, J., Lundin, N., Haggman, M., and Malmstrom, P. U. Positron emission tomography with C11-acetate for tumor detection and localization in patients with prostate-specific antigen relapse after radical prostatectomy. *Urology*, **2006,** 67(5), 996-1000.
40. Wachter, S., Tomek, S., Kurtaran, A., Wachter-Gerstner, N., Djavan, B., Becherer, A., Mitterhauser, M., Dobrozemsky, G., Li, S., Potter, R., Dudczak, R., and Kletter, K. 11C-acetate positron emission tomography imaging and image fusion with computed tomography and magnetic resonance imaging in patients with recurrent prostate cancer. *J Clin Oncol*, **2006,** 24(16), 2513-2519.
41. Oyama, N., Akino, H., Kanamaru, H., Suzuki, Y., Muramoto, S., Yonekura, Y., Sadato, N., Yamamoto, K., and Okada, K. 11C-acetate PET imaging of prostate cancer. *J Nucl Med*, **2002,** 43(2), 181-186.
42. Kotzerke, J., Volkmer, B. G., Neumaier, B., Gschwend, J. E., Hautmann, R. E., and Reske, S. N. Carbon-11 acetate positron emission tomography can detect local recurrence of prostate cancer. *Eur J Nucl Med Mol Imaging*, **2002,** 29(10), 1380-1384.
43. Fusi, A., Procopio, G., Della Torre, S., Ricotta, R., Bianchini, G., Salvioni, R., Ferrari, L., Martinetti, A., Savelli, G., Villa, S., and Bajetta, E. Treatment options in hormone-refractory metastatic prostate carcinoma. *Tumori*, **2004,** 90(6), 535-546.
44. Scher, H. I., and Sawyers, C. L. Biology of progressive, castration-resistant prostate cancer: directed therapies targeting the androgen-receptor signaling axis. *J Clin Oncol*, **2005,** 23(32), 8253-8261.
45. Stephenson, A. J., Shariat, S. F., Zelefsky, M. J., Kattan, M. W., Butler, E. B., Teh, B. S., Klein, E. A., Kupelian, P. A., Roehrborn, C. G., Pistenmaa, D. A., Pacholke, H. D., Liauw, S. L., Katz, M. S., Leibel, S. A., Scardino, P. T., and Slawin, K. M. Salvage radiotherapy for recurrent prostate cancer after radical prostatectomy. *JAMA*, **2004,** 291(11), 1325-1332.
46. Oyama, N., Kim, J., Jones, L. A., Mercer, N. M., Engelbach, J. A., Sharp, T. L., and Welch, M. J. MicroPET assessment of androgenic control of glucose and acetate uptake in the rat prostate and a prostate cancer tumor model. *Nucl Med Biol*, **2002,** 29(8), 783-790.
47. Mueller-Lisse, U. G., Swanson, M. G., Vigneron, D. B., Hricak, H., Bessette, A., Males, R. G., Wood, P. J., Noworolski, S., Nelson, S. J., Barken, I., Carroll, P. R., and Kurhanewicz, J. Time-dependent effects of hormone-deprivation therapy on prostate metabolism as detected by combined magnetic resonance imaging and 3D magnetic resonance spectroscopic imaging. *Magn Reson Med*, **2001,** 46(1), 49-57.
48. Seltzer, M. A., Barbaric, Z., Belldegrun, A., Naitoh, J., Dorey, F., Phelps, M. E., Gambhir, S. S., and Hoh, C. K. Comparison of helical computerized tomography, positron emission tomography and monoclonal antibody scans for evaluation of lymph node metastases in patients with prostate specific antigen relapse after treatment for localized prostate cancer. *J Urol*, **1999,** 162(4), 1322-1328.

49. Shurbaji, M. S., Kuhajda, F. P., Pasternack, G. R., and Thurmond, T. S. Expression of oncogenic antigen 519 (OA-519) in prostate cancer is a potential prognostic indicator. *Am J Clin Pathol*, **1992,** 97(5), 686-691.
50. Shurbaji, M. S., Kalbfleisch, J. H., and Thurmond, T. S. Immunohistochemical detection of a fatty acid synthase (OA-519) as a predictor of progression of prostate cancer. *Hum Pathol*, **1996,** 27(9), 917-921.
51. Epstein, J. I., Carmichael, M., and Partin, A. W. OA-519 (fatty acid synthase) as an independent predictor of pathologic state in adenocarcinoma of the prostate. *Urology*, **1995,** 45(1), 81-86.
52. Vavere, A. L., Kridel, S. J., Wheeler, F. B., and Lewis, J. S. 1-11C-acetate as a PET radiopharmaceutical for imaging fatty acid synthase expression in prostate cancer. *J Nucl Med*, **2008,** 49(2), 327-334.
53. Ohtsuka, T., Nomori, H., Watanabe, K., Naruke, T., Suemasu, K., Kosaka, N., and Uno, K. Positive imaging of thymoma by 11C-acetate positron emission tomography. *Ann Thorac Surg*, **2006,** 81(3), 1132-1134.
54. Shriki, J., Murthy, V., and Brown, J. Renal oncocytoma on 1-11C acetate positron emission tomography: Case report and literature review. *Mol Imaging Biol*, **2006,** 8(4), 208-211.
55. Higashi, K., Ueda, Y., Matsunari, I., Kodama, Y., Ikeda, R., Miura, K., Taki, S., Higuchi, T., Tonami, H., and Yamamoto, I. 11C-acetate PET imaging of lung cancer: comparison with 18F-FDG PET and 99mTc-MIBI SPET. *Eur J Nucl Med Mol Imaging*, **2004,** 31(1), 13-21.
56. Weber, G., and Morris, H. P. Comparative Biochemistry of Hepatomas. Iii. Carbohydrate Enzymes in Liver Tumors of Different Growth Rates. *Cancer Res*, **1963,** 23(987-994.
57. Sakurai, H., Kaji, M., and Suemasu, K. Thymoma of the middle mediastinum: 11C-acetate positron emission tomography imaging. *Ann Thorac Surg*, **2009,** 87(4), 1271-1274.
58. Evert, M., Schneider-Stock, R., and Dombrowski, F. Overexpression of fatty acid synthase in chemically and hormonally induced hepatocarcinogenesis of the rat. *Lab Invest*, **2005,** 85(1), 99-108.
59. Horiguchi, A., Asano, T., Ito, K., Sumitomo, M., and Hayakawa, M. Fatty acid synthase over expression is an indicator of tumor aggressiveness and poor prognosis in renal cell carcinoma. *J Urol*, **2008,** 180(3), 1137-1140.
60. Prenen, H., Deroose, C., Vermaelen, P., Sciot, R., Debiec-Rychter, M., Stroobants, S., Mortelmans, L., Schoffski, P., and Van Oosterom, A. Establishment of a mouse gastrointestinal stromal tumour model and evaluation of response to imatinib by small animal positron emission tomography. *Anticancer Res*, **2006,** 26(2A), 1247-1252.
61. Van den Abbeele, A. D. The lessons of GIST--PET and PET/CT: a new paradigm for imaging. *Oncologist*, **2008,** 13 Suppl 2(8-13.
62. Engelman, J. A., Chen, L., Tan, X., Crosby, K., Guimaraes, A. R., Upadhyay, R., Maira, M., McNamara, K., Perera, S. A., Song, Y., Chirieac, L. R., Kaur, R., Lightbown, A., Simendinger, J., Li, T., Padera, R. F., Garcia-Echeverria, C., Weissleder, R., Mahmood, U., Cantley, L. C., and Wong, K. K. Effective use of PI3K and MEK inhibitors to treat mutant Kras G12D and PIK3CA H1047R murine lung cancers. *Nat Med*, **2008,** 14(12), 1351-1356.
63. Funabashi, H., Kawaguchi, A., Tomoda, H., Omura, S., Okuda, S., and Iwasaki, S. Binding site of cerulenin in fatty acid synthetase. *J Biochem*, **1989,** 105(5), 751-755.
64. Pizer, E. S., Jackisch, C., Wood, F. D., Pasternack, G. R., Davidson, N. E., and Kuhajda, F. P. Inhibition of fatty acid synthesis induces programmed cell death in human breast cancer cells. *Cancer Res*, **1996,** 56(12), 2745-2747.
65. Kuhajda, F. P., Pizer, E. S., Li, J. N., Mani, N. S., Frehywot, G. L., and Townsend, C. A. Synthesis and antitumor activity of an inhibitor of fatty acid synthase. *Proc Natl Acad Sci U S A*, **2000,** 97(7), 3450-3454.

66. Alli, P. M., Pinn, M. L., Jaffee, E. M., McFadden, J. M., and Kuhajda, F. P. Fatty acid synthase inhibitors are chemopreventive for mammary cancer in neu-N transgenic mice. *Oncogene*, **2005,** 24(1), 39-46.
67. Zhou, W., Han, W. F., Landree, L. E., Thupari, J. N., Pinn, M. L., Bililign, T., Kim, E. K., Vadlamudi, A., Medghalchi, S. M., El Meskini, R., Ronnett, G. V., Townsend, C. A., and Kuhajda, F. P. Fatty acid synthase inhibition activates AMP-activated protein kinase in SKOV3 human ovarian cancer cells. *Cancer Res*, **2007,** 67(7), 2964-2971.
68. Kridel, S. J., Axelrod, F., Rozenkrantz, N., and Smith, J. W. Orlistat is a novel inhibitor of fatty acid synthase with antitumor activity. *Cancer Res*, **2004,** 64(6), 2070-2075.
69. Pemble, C. W. t., Johnson, L. C., Kridel, S. J., and Lowther, W. T. Crystal structure of the thioesterase domain of human fatty acid synthase inhibited by Orlistat. *Nat Struct Mol Biol*, **2007,** 14(8), 704-709.
70. Richardson, R. D., Ma, G., Oyola, Y., Zancanella, M., Knowles, L. M., Cieplak, P., Romo, D., and Smith, J. W. Synthesis of novel beta-lactone inhibitors of fatty acid synthase. *J Med Chem*, **2008,** 51(17), 5285-5296.
71. Zhang, W., Richardson, R. D., Chamni, S., Smith, J. W., and Romo, D. Beta-lactam congeners of orlistat as inhibitors of fatty acid synthase. *Bioorg Med Chem Lett*, **2008,** 18(7), 2491-2494.
72. Richardson, R. D., and Smith, J. W. Novel antagonists of the thioesterase domain of human fatty acid synthase. *Mol Cancer Ther*, **2007,** 6(7), 2120-2126.
73. Liu, Y., Tian, W., Ma, X., and Ding, W. Evaluation of inhibition of fatty acid synthase by ursolic acid: positive cooperation mechanism. *Biochem Biophys Res Commun*, **2010,** 392(3), 386-390.
74. Tian, W. X. Inhibition of fatty acid synthase by polyphenols. *Curr Med Chem*, **2006,** 13(8), 967-977.
75. Vazquez, M. J., Leavens, W., Liu, R., Rodriguez, B., Read, M., Richards, S., Winegar, D., and Dominguez, J. M. Discovery of GSK837149A, an inhibitor of human fatty acid synthase targeting the beta-ketoacyl reductase reaction. *FEBS J*, **2008,** 275(7), 1556-1567.
76. Chakravarty, B., Gu, Z., Chirala, S. S., Wakil, S. J., and Quiocho, F. A. Human fatty acid synthase: structure and substrate selectivity of the thioesterase domain. *Proc Natl Acad Sci U S A*, **2004,** 101(44), 15567-15572.
77. Pappenberger, G., Benz, J., Gsell, B., Hennig, M., Ruf, A., Stihle, M., Thoma, R., and Rudolph, M. G. Structure of the human fatty acid synthase KS-MAT didomain as a framework for inhibitor design. *J Mol Biol*, **2010,** 397(2), 508-519.
78. Lee, J. S., Orita, H., Gabrielson, K., Alvey, S., Hagemann, R. L., Kuhajda, F. P., Gabrielson, E., and Pomper, M. G. FDG-PET for pharmacodynamic assessment of the fatty acid synthase inhibitor C75 in an experimental model of lung cancer. *Pharm Res*, **2007,** 24(6), 1202-1207.
79. Swinnen, J. V., Vanderhoydonc, F., Elgamal, A. A., Eelen, M., Vercaeren, I., Joniau, S., Van Poppel, H., Baert, L., Goossens, K., Heyns, W., and Verhoeven, G. Selective activation of the fatty acid synthesis pathway in human prostate cancer. *Int J Cancer*, **2000,** 88(2), 176-179.
80. Yahagi, N., Shimano, H., Hasegawa, K., Ohashi, K., Matsuzaka, T., Najima, Y., Sekiya, M., Tomita, S., Okazaki, H., Tamura, Y., Iizuka, Y., Nagai, R., Ishibashi, S., Kadowaki, T., Makuuchi, M., Ohnishi, S., Osuga, J., and Yamada, N. Co-ordinate activation of lipogenic enzymes in hepatocellular carcinoma. *Eur J Cancer*, **2005,** 41(9), 1316-1322.
81. Yoon, S., Lee, M. Y., Park, S. W., Moon, J. S., Koh, Y. K., Ahn, Y. H., Park, B. W., and Kim, K. S. Up-regulation of acetyl-CoA carboxylase alpha and fatty acid synthase by human epidermal growth factor receptor 2 at the translational level in breast cancer cells. *J Biol Chem*, **2007,** 282(36), 26122-26131.

82. Milgraum, L. Z., Witters, L. A., Pasternack, G. R., and Kuhajda, F. P. Enzymes of the fatty acid synthesis pathway are highly expressed in in situ breast carcinoma. *Clin Cancer Res*, **1997,** 3(11), 2115-2120.
83. Corbett, J. W. Review of recent acetyl-CoA carboxylase inhibitor patents: mid-2007-2008. *Expert Opin Ther Pat*, **2009,** 19(7), 943-956.
84. McCune, S. A., and Harris, R. A. Mechanism responsible for 5-(tetradecyloxy)-2-furoic acid inhibition of hepatic lipogenesis. *J Biol Chem*, **1979,** 254(20), 10095-10101.
85. Wang, C., Xu, C., Sun, M., Luo, D., Liao, D. F., and Cao, D. Acetyl-CoA carboxylase-alpha inhibitor TOFA induces human cancer cell apoptosis. *Biochem Biophys Res Commun*, **2009,** 385(3), 302-306.
86. Thupari, J. N., Pinn, M. L., and Kuhajda, F. P. Fatty acid synthase inhibition in human breast cancer cells leads to malonyl-CoA-induced inhibition of fatty acid oxidation and cytotoxicity. *Biochem Biophys Res Commun*, **2001,** 285(2), 217-223.
87. Beckers, A., Organe, S., Timmermans, L., Scheys, K., Peeters, A., Brusselmans, K., Verhoeven, G., and Swinnen, J. V. Chemical inhibition of acetyl-CoA carboxylase induces growth arrest and cytotoxicity selectively in cancer cells. *Cancer Res*, **2007,** 67(17), 8180-8187.
88. Harwood, H. J., Jr., Petras, S. F., Shelly, L. D., Zaccaro, L. M., Perry, D. A., Makowski, M. R., Hargrove, D. M., Martin, K. A., Tracey, W. R., Chapman, J. G., Magee, W. P., Dalvie, D. K., Soliman, V. F., Martin, W. H., Mularski, C. J., and Eisenbeis, S. A. Isozyme-nonselective N-substituted bipiperidylcarboxamide acetyl-CoA carboxylase inhibitors reduce tissue malonyl-CoA concentrations, inhibit fatty acid synthesis, and increase fatty acid oxidation in cultured cells and in experimental animals. *J Biol Chem*, **2003,** 278(39), 37099-37111.
89. Mao, J., DeMayo, F. J., Li, H., Abu-Elheiga, L., Gu, Z., Shaikenov, T. E., Kordari, P., Chirala, S. S., Heird, W. C., and Wakil, S. J. Liver-specific deletion of acetyl-CoA carboxylase 1 reduces hepatic triglyceride accumulation without affecting glucose homeostasis. *Proc Natl Acad Sci U S A*, **2006,** 103(22), 8552-8557.
90. Abu-Elheiga, L., Matzuk, M. M., Abo-Hashema, K. A., and Wakil, S. J. Continuous fatty acid oxidation and reduced fat storage in mice lacking acetyl-CoA carboxylase 2. *Science*, **2001,** 291(5513), 2613-2616.
91. Ha, J., Daniel, S., Broyles, S. S., and Kim, K. H. Critical phosphorylation sites for acetyl-CoA carboxylase activity. *J Biol Chem*, **1994,** 269(35), 22162-22168.
92. Gaidhu, M. P., Fediuc, S., and Ceddia, R. B. 5-Aminoimidazole-4-carboxamide-1-beta-D-ribofuranoside-induced AMP-activated protein kinase phosphorylation inhibits basal and insulin-stimulated glucose uptake, lipid synthesis, and fatty acid oxidation in isolated rat adipocytes. *J Biol Chem*, **2006,** 281(36), 25956-25964.
93. Wright, J. L., and Stanford, J. L. Metformin use and prostate cancer in Caucasian men: results from a population-based case-control study. *Cancer Causes Control*, **2009,** 20(9), 1617-1622.
94. Maleddu, A., Pantaleo, M. A., Castellucci, P., Astorino, M., Nanni, C., Nannini, M., Busato, F., Di Battista, M., Farsad, M., Lodi, F., Boschi, S., Fanti, S., and Biasco, G. 11C-acetate PET for early prediction of sunitinib response in metastatic renal cell carcinoma. *Tumori*, **2009,** 95(3), 382-384.
95. Demoulin, J. B., Ericsson, J., Kallin, A., Rorsman, C., Ronnstrand, L., and Heldin, C. H. Platelet-derived growth factor stimulates membrane lipid synthesis through activation of phosphatidylinositol 3-kinase and sterol regulatory element-binding proteins. *J Biol Chem*, **2004,** 279(34), 35392-35402.
96. Van de Sande, T., De Schrijver, E., Heyns, W., Verhoeven, G., and Swinnen, J. V. Role of the phosphatidylinositol 3'-kinase/PTEN/Akt kinase pathway in the overexpression of fatty acid synthase in LNCaP prostate cancer cells. *Cancer Res*, **2002,** 62(3), 642-646.

97. Wang, H. Q., Altomare, D. A., Skele, K. L., Poulikakos, P. I., Kuhajda, F. P., Di Cristofano, A., and Testa, J. R. Positive feedback regulation between AKT activation and fatty acid synthase expression in ovarian carcinoma cells. *Oncogene*, **2005,** 24(22), 3574-3582.
98. Garlich, J. R., De, P., Dey, N., Su, J. D., Peng, X., Miller, A., Murali, R., Lu, Y., Mills, G. B., Kundra, V., Shu, H. K., Peng, Q., and Durden, D. L. A vascular targeted pan phosphoinositide 3-kinase inhibitor prodrug, SF1126, with antitumor and antiangiogenic activity. *Cancer Res*, **2008,** 68(1), 206-215.
99. Howes, A. L., Chiang, G. G., Lang, E. S., Ho, C. B., Powis, G., Vuori, K., and Abraham, R. T. The phosphatidylinositol 3-kinase inhibitor, PX-866, is a potent inhibitor of cancer cell motility and growth in three-dimensional cultures. *Mol Cancer Ther*, **2007,** 6(9), 2505-2514.
100. Yang, Y. A., Han, W. F., Morin, P. J., Chrest, F. J., and Pizer, E. S. Activation of fatty acid synthesis during neoplastic transformation: role of mitogen-activated protein kinase and phosphatidylinositol 3-kinase. *Exp Cell Res*, **2002,** 279(1), 80-90.
101. Shah, U. S., Dhir, R., Gollin, S. M., Chandran, U. R., Lewis, D., Acquafondata, M., and Pflug, B. R. Fatty acid synthase gene overexpression and copy number gain in prostate adenocarcinoma. *Hum Pathol*, **2006,** 37(4), 401-409.
102. Graner, E., Tang, D., Rossi, S., Baron, A., Migita, T., Weinstein, L. J., Lechpammer, M., Huesken, D., Zimmermann, J., Signoretti, S., and Loda, M. The isopeptidase USP2a regulates the stability of fatty acid synthase in prostate cancer. *Cancer Cell*, **2004,** 5(3), 253-261.
103. Swinnen, J. V., Esquenet, M., Goossens, K., Heyns, W., and Verhoeven, G. Androgens stimulate fatty acid synthase in the human prostate cancer cell line LNCaP. *Cancer Res*, **1997,** 57(6), 1086-1090.
104. Lakshmanan, M. R., Nepokroeff, C. M., and Porter, J. W. Control of the synthesis of fatty-acid synthetase in rat liver by insulin, glucagon, and adenosine 3':5' cyclic monophosphate. *Proc Natl Acad Sci U S A*, **1972,** 69(12), 3516-3519.
105. Schmidt, L. J., Ballman, K. V., and Tindall, D. J. Inhibition of fatty acid synthase activity in prostate cancer cells by dutasteride. *Prostate*, **2007,** 67(10), 1111-1120.
106. Ponde, D. E., Dence, C. S., Oyama, N., Kim, J., Tai, Y. C., Laforest, R., Siegel, B. A., and Welch, M. J. 18F-fluoroacetate: a potential acetate analog for prostate tumor imaging--in vivo evaluation of 18F-fluoroacetate versus 11C-acetate. *J Nucl Med*, **2007,** 48(3), 420-428.
107. Wellen, K. E., Hatzivassiliou, G., Sachdeva, U. M., Bui, T. V., Cross, J. R., and Thompson, C. B. ATP-citrate lyase links cellular metabolism to histone acetylation. *Science*, **2009,** 324(5930), 1076-1080.
108. Hager, M. H., Solomon, K. R., and Freeman, M. R. The role of cholesterol in prostate cancer. *Curr Opin Clin Nutr Metab Care*, **2006,** 9(4), 379-385.
109. Therasse, P., Arbuck, S. G., Eisenhauer, E. A., Wanders, J., Kaplan, R. S., Rubinstein, L., Verweij, J., Van Glabbeke, M., van Oosterom, A. T., Christian, M. C., and Gwyther, S. G. New guidelines to evaluate the response to treatment in solid tumors. European Organization for Research and Treatment of Cancer, National Cancer Institute of the United States, National Cancer Institute of Canada. *J Natl Cancer Inst*, **2000,** 92(3), 205-216.
110. Twombly, R. Criticism of tumor response criteria raises trial design questions. *J Natl Cancer Inst*, **2006,** 98(4), 232-234.